Photoacoustics 20 (2020) 100211

Contents lists available at ScienceDirect

Photoacoustics

journal homepage: www.elsevier.com/locate/pacs

Photoacoustic imaging with fiber optic technology: A review

Jingcheng Zhou [a], Jesse V. Jokerst [a,b,c,*]

[a] Department of NanoEngineering, University of California, San Diego, 9500 Gilman Drive, La Jolla, CA 92092, USA
[b] Materials Science and Engineering Program, University of California, San Diego, 9500 Gilman Drive, La Jolla, CA 92092, USA
[c] Department of Radiology, University of California, San Diego, 9500 Gilman Drive, La Jolla, CA 92092, USA

ARTICLE INFO

Keywords:
Photoacoustic imaging
Fiber optic
Ultrasound
Biosensors

ABSTRACT

Photoacoustic imaging (PAI) has achieved remarkable growth in the past few decades since it takes advantage of both optical and ultrasound (US) imaging. In order to better promote the wide clinical applications of PAI, many miniaturized and portable PAI systems have recently been proposed. Most of these systems utilize fiber optic technologies. Here, we overview the fiber optic technologies used in PAI. This paper discusses three different fiber optic technologies: fiber optic light transmission, fiber optic US transmission, and fiber optic US detection. These fiber optic technologies are analyzed in different PAI modalities including photoacoustic microscopy (PAM), photoacoustic computed tomography (PACT), and minimally invasive photoacoustic imaging (MIPAI).

1. Introduction

Optical imaging can be a powerful tool for diagnosing and treating human diseases in healthcare but tissue is a highly scattering medium. Due to this optical scattering, conventional optical imaging methods cannot provide high-resolution imaging in deep biological tissues [1]. However, optical signals in tissue can be transferred into ultrasound (US) signals, which are scattered much less. Photoacoustic imaging (PAI) is a hybrid imaging modality that combines the advantages of optical imaging and ultrasound imaging [2–5]. PA signals come from optical absorption. In PAI, pulsed or amplitude-modulated optical energy is delivered to imaging target. Some PAI systems deliver light energy to the tissue surface, while other PAI systems deliver light energy to the inside of the tissue through optical fibers [6–15]. The delivered optical energy will be absorbed and converted into heat, which will cause transient thermoelastic expansion and lead to broadband ultrasound emission. The generated photoacoustic pressure propagates through the medium and is detected by an ultrasonic transducer or transducer array at multiple sites. [16–20]. PAI can provide deeper imaging depth and higher spatial resolution than conventional optical imaging methods because the scattering of the ultrasonic signal by physiological tissue is 2–3 orders of magnitude lower than the optical signal. PAI can also provide higher contrast between different tissues than ultrasound because the contrast depends on optical absorption versus the mechanical and elastic properties of the tissue [21–35].

1.1. PAI implementations

Currently, PAI can be classified into PA microscopy (PAM), PA computed tomography (PACT), and minimally invasive PA imaging (MIPAI) based on the target imaging depth [36] as shown in Fig. 1. PAM employs focused optical illumination and focused acoustic detection (Fig. 1), which can achieve high spatial resolution (<50 μm) but low imaging depth (<10 mm). PACT employs wide-field optical illumination and unfocused acoustic detection (Fig. 1) providing relatively low spatial resolution (>50 μm) but relatively high imaging depth (10−100 mm) [37,38]. MIPAI employs internal optical illumination (Fig. 1) providing the deepest imaging depth (>100 mm) of these three categories. The spatial resolution and the imaging depth information relationship for PAI is shown in Fig. 1(b) [36].

PAM can be further categorized as optical resolution PAM (OR-PAM) and acoustic resolution PAM (AR-PAM) based on the spatial resolution (Fig. 1). In OR-PAM, the optical focus is much tighter than acoustic focus, while in AR-PAM, the acoustic focus is tighter than the scattered beam as shown in Fig. 1 [36]. Consequently, OR-PAM imaging depth (<1 mm) is limited by optical diffusion but can achieve a high lateral resolution (<10 μm). Conversely, AR-PAM imaging depth (1−10 mm) is determined by acoustic focus but providing relatively low lateral resolution (<50 μm) compared to OR-PAM [36,38,39]. In summary, AR-PAM systems usually have lower lateral resolution com-pared to OR-PAM but higher depth of penetration. In both cases, the axial resolution is determined by the bandwidth of the ultrasonic transducer. The

* Corresponding author at: Department of NanoEngineering, University of California, San Diego, 9500 Gilman Drive, La Jolla, CA 92092, USA.
E-mail address: jjokerst@ucsd.edu (J.V. Jokerst).

https://doi.org/10.1016/j.pacs.2020.100211
Received 28 May 2020; Received in revised form 5 September 2020; Accepted 19 September 2020
Available online 22 October 2020

detection image is formed by mechanically scanning the optical/acoustic focus point and then simply combining the scanned signal.

In PACT, wide-field high-energy light is irradiated on the tis-sue surface to generate photoacoustic waves that are detect-ed by wide-band ultrasonic transducers. These ultrasonic transducers can be either a single ultrasonic transducer rotating around the sample, a linear array of transducer elements, or a fixed ring array of multiple transducer elements [40]. As a result, PACT offers higher imaging depth (10−100 mm) and lower spatial resolution (>50 μm) than PAM. The detection image is normally formed through digital image reconstruction algorithms [38].

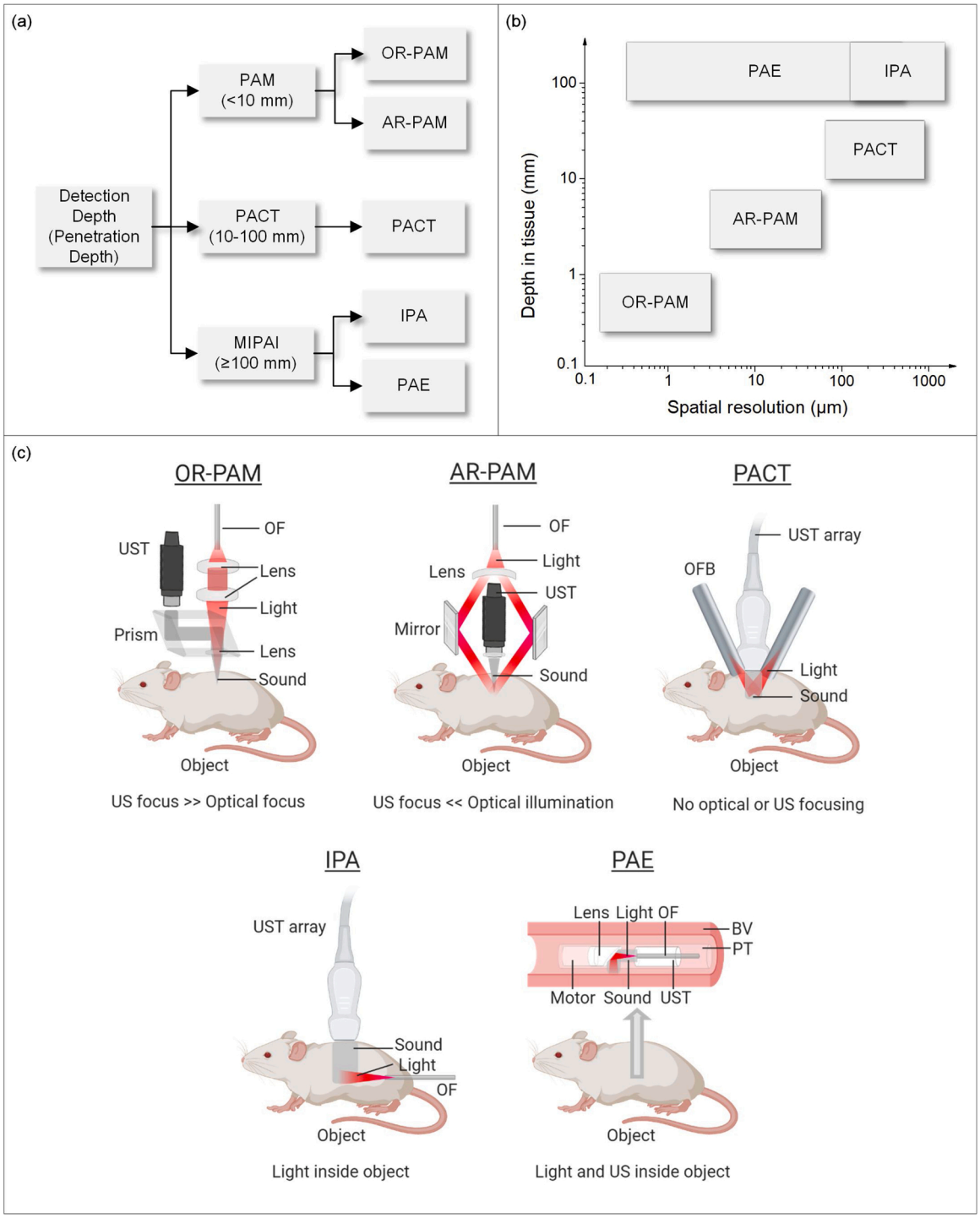

Fig. 1. Photoacoustic imaging implementation. (a) Photoacoustic imaging implementation based on detection depth. PAI, photoacoustic imaging; PAM, photoacoustic microscopy; PACT, photoacoustic computed tomography; MIPAI, minimally invasive photoacoustic imaging; OR-PAM, optical resolution photoacoustic microscopy; AR-PAM, acoustic resolution photoacoustic microscopy; IPA, internal-illumination photoacoustic; PAE, Photoacoustic endoscopy. (b) Spatial resolution versus depth of examinations for photoacoustic imaging (PAI) techniques. OR-PAM, optical resolution photoacoustic microscopy; AR-PAM, acoustic resolution photoacoustic microscopy; PACT, photoacoustic computed tomography; IPA, internal-illumination photoacoustic; IPA, internal-illumination photoacoustic; PAE, Photoacoustic endoscopy [36]. (c) Representative implementations of fiber optic-based photoacoustic imaging. OR-PAM, optical resolution photoacoustic microscopy; AR-PAM, acoustic resolution photoacoustic microscopy; PACT, photoacoustic computed tomography; IPA, internal-illumination photoacoustic; PAE, Photoacoustic endoscopy; OF, optical fiber; UST, ultrasound transducer; OFB, optical fiber bundle; BV, blood vessel; PT, protection tube.

Due to the strong attenuation of photons, the maximum tissue depth at which PAM and PACT can achieve sufficient contrast from endogenous chromophores has been limited to 40 mm [41]. The deepest penetration depth for PACT and PAM reported is 120 mm in chicken breast tissue using highly absorbing exogenous contrast agent surfactant-stripped CyFaP (ss-CyFaP) [42]. Clinical applications include prostate and breast imaging. The prostate is located more than 100 mm from the skin surface. To deal with these deep internal tissue applications, minimally invasive PA imaging (MIPAI) has been developed in recent years [43–48]. Compared to traditional non-invasive PAI techniques, MIPAI techniques utilize fiber optic technologies to deliver light inside of the body for imaging [49–63].

MIPAI systems have been built in various clinical fields, including fetal surgery [45], deep brain imaging [64], prostate cancer imaging [65–67], interventional guidance radiofrequency ablation on liver [68], gastrointestinal tract imaging [69–71], vascular network imaging [72], cervical cancer diagnostic [73], and so on. In these systems, the optical fiber light delivery component is set in the instrument channel of the interventional medical equipment [36]. The PA signal detection component is arranged on the surface of the tissue or in the body.

Based on the installation position of the ultrasonic transducer, MIPAI can be divided into internal-illumination photoacoustic (IPA) and photoacoustic endoscopes (PAE) as shown in Fig. 1 [36]. In IPA, the ultrasonic transducer is placed outside the body. In contrast, in PAE, the ultrasonic transducer is in the body. Since the light source can set inside the body, the imaging depth (>100 mm) of IPA and PAE usually is highest among all these categories. The spatial resolution of both cases is determined ultrasonic transducer properties. Most MIPAI detection images are usually produced by digital image reconstruction algorithms.

1.2. Fiber optic technology in PAI

Fiber optic technology are broadly used in PAI [74–76]. The uses of fiber optics in PAI are mainly divided into the following three types, light transmission [77–79], US transmission [80], and US detection [81] as shown in Fig. 2(a). In PAI, the main function of fiber optics is to transmit light to imaging targets. In some cases of PAM or PACT, a single fiber or a fiber bundle is used to transfer light from the light source to the tissue surface [82]. The benefit of this fiber optic structure is that people can more easily move the light to imaging targets. In MIPAI, fiber optic light transmission technology is used in almost all cases. Due to the need to transmit light into the body, optical fibers have become the best light carrier [83].

Another type of fiber optic technology used in PAI is fiber optic US transmission technology. Recently, photoacoustic ultrasound excitation technology is increasingly used for biomedical intravascular imaging [84]. Different from traditional PAI, the exogenous contrast agent is directly coated on the optical fiber so that the optical fiber can generate US signals. The exogenous contrast agent can be carbon black with Polydimethylsiloxane (PDMS) [85], Graphite with epoxy resin [86], carbon nanotubes (CNTs) with PDMS [87], and carbon nanofibers with PDMS [88] as well as gold nano-composite [89,90]. This fiber optic US transmission technology is mostly used in MIPAI. This fiber optic US probe can generate broadband wide-angle US signals and can provide image contrast complementary to traditional PAI. This imaging modality can also be recognized as US imaging based on the principle of the PA effect. Fig. 2 (b) shows the different mechanisms of contrast for the traditional PAI and the PA based US. In traditional PAI, the incident light generated PA signal in the subject. This signal propagates back to a detector. In PA-based US, the PA effect is localized on the tip of the fiber for pulse-echo imaging.

The last category of fiber optic technology broadly used in PAI is fiber optic US detection technology. The optical fiber is used as the ultrasonic transducer to detect the signals. This kind of fiber optic US detection sensor features high sensitivity, small size, easy fabrication, low cost, and survived in a harsh environment compared to the

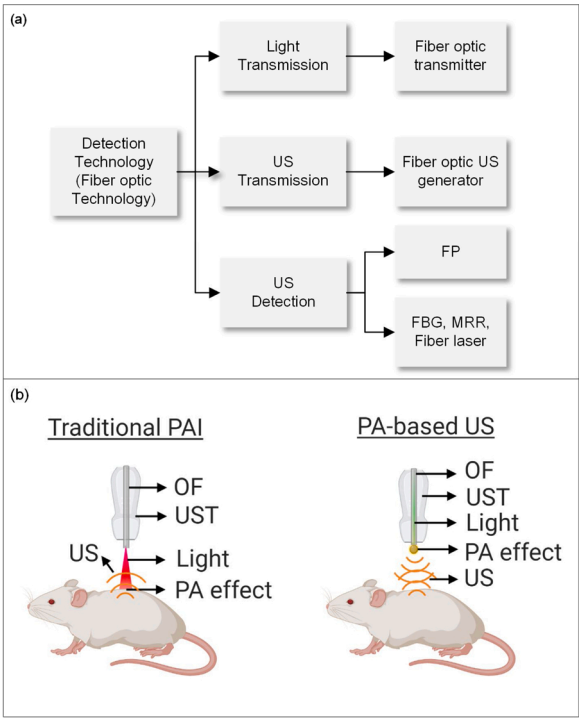

Fig. 2. (a) Fiber optic technology in PAI. FP, fiber optic Fabry-Perot technology; FBG, fiber Bragg grating technology; MRR, micro-ring resonator technology. (b) Representative implementations of traditional photoacoustic imaging and photoacoustic based ultrasound. PAI, photoacoustic imaging; OF, optical fiber; UST, ultrasound transducer; PA, photoacoustic; US, ultrasound. In traditional PAI, the incident light generated PA signal in the subject. This signal propagates back to a detector. In PA-based US, the PA effect is localized on the tip of the fiber for pulse-echo imaging.

electronic ultrasonic transducer. The main part of the fiber optic US detection technology is based on fiber optics Fabry-Perot (FP) principle [91]. There is a sandwich structure FP interferometer fabricated on the tip of the fiber. Different materials are used to manufacture this sandwich structure, such as epoxy, Parylene C, PDMS, and so on [92]. The fiber optic FP technology is usually used in PAE. Other types of fiber optic US detection technology are also used in PAI, such as Fiber Bragg Grating (FBG) technology, Micro-Ring Resonator (MRR) technology, fiber laser technology and so on [93,94]. These technologies are mostly used in PAM and PACT.

The structure of this review is as follows: Section 2 reviews fiber optic light transmission technology. Section 3 reviews fiber optic US transmission technology. Section 4 reviews fiber optic US detection technology. Finally, in Section 5, some conclusions on all these fiber optic technology for PAI are discussed.

2. Fiber optic light transmission

2.1. Light transmission in PAM and PACT

In PAI, fiber optic technology is primarily used to transmit light to imaging targets because of its flexibility and compactness. In PAM and PACT, single mode fiber (SMF), multimode fiber (MMF), and optical fiber bundles all can be used for light transmission.

The conventional PAM system utilizes a mechanical raster scanning mechanism with motorized stages. The system is bulky and inherently slow in imaging speed, limiting its wide-spread use in preclinical and clinical research. Recently, the SMF is widely used in portable handheld PAM. Park et al. [95] developed a PAM system using an SMF to transmit light (Fig. 3(a)). In their design, beams from a Q-switched pulsed laser were coupled into an SMF for convenient light delivery. The light was

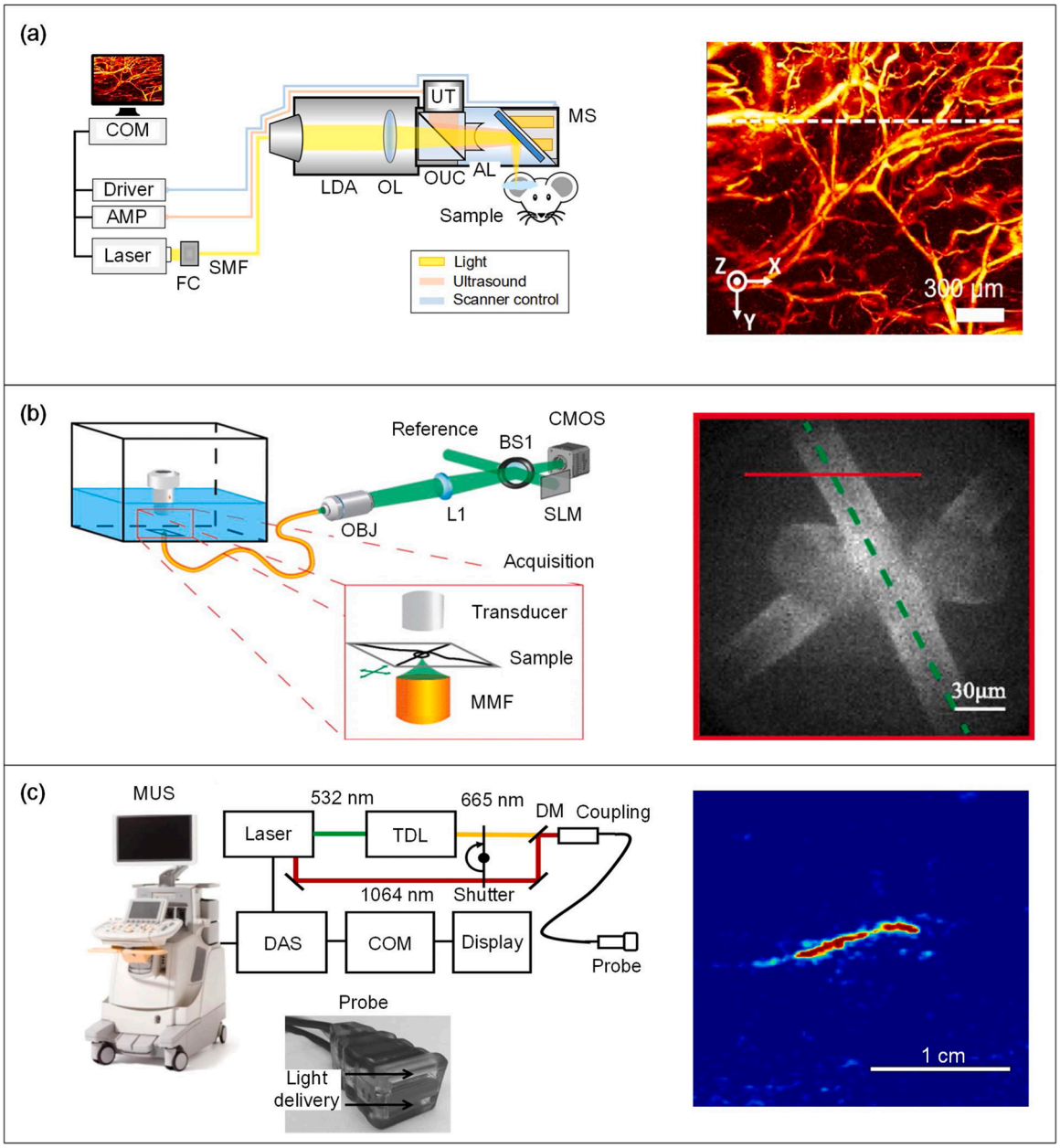

Fig. 3. Embodiments of fiber optic light transmission technology in PAM and PACT. (a) Schematic of the handheld PAM probe system based on an SMF; In vivo PAM image of micro-vasculature in a mouse ear. AL, acoustic lens; AMP, amplifier; AT, adjustable tube; CL, collimation lens; COM, computer; EM, electromagnets; FC, fiber collimator; LDA, light delivery assembly; MR, mirror; MS, MEMS scanner; OL, objective lens; OUC, opto-ultrasound combiner; SMF, single mode fiber; UT, ultrasonic transducer; WT, water tank. Reprinted and adapted with permission from ref [95]. (b) Schematic of the experimental setup for the generation of PAM images using an MMF for the optical excitation; PAM image of knot immersed in water. MMF, multimode fiber; CMOS, complementary metal oxide semiconductor camera; BS1, beam splitter; SLM, spatial light modulator; L1, tube lens; OBJ, objective. Reprinted and adapted with permission from ref [96]. (c) Schematic of the PACT system and photograph of the probe; In vivo PCAT image of methylene blue dye. TDL, tunable dye laser; DM, dichroic mirror; COM, computer; DAS, data acquisition system; MUS, modified ultrasound system. Reprinted and adapted with permission from ref [97]. (For interpretation of the references to colour in this figure legend, the reader is referred to the web version of this article).

transmitted to a handheld PAM probe. This handheld probe based on microelectromechanical systems (MEMS) technology. This probe's advantages are its compact size, large imaging range and fast imaging speed: diameter of 17 mm, weight of 162 g, maximum imaging range of 3 mm × 4 mm, and an imaging speed of 35 Hz. However, fiber coupling may be difficult due to the SMF use, and the output optical energy is relatively small.

The MMF is easier to couple than the SMF and are less susceptible to damage due to good coupling. The MMF can transmit more light energy than the SMF. Papadopoulos et al. [96] built a PAM system using an MMF, as shown in Fig. 3(b). The optical field that propagates through the fiber couples to the different modes may cause the output light scram-bled. In their system, an optical phase conjugation technology has been used to eliminate the scattering. A Q-switched pulse laser light was focused on the diffraction limit point by the microscope objective (OBJ), and then propagated through the MMF to the proximal tip, and a spot pattern was generated at the proximal tip. The reference beam was modulated by the spatial light modulator (SLM) forming the optical phase conjugate beam. The system has high resolution with a resolution of 1.5 μm, but its microscopic field of view is limited with a field-of-view

of 201 μm × 201 μm.

Different from the focused light in PAM, PACT is based on wide-area light illumination. Optical fiber bundles have become a better candidate in PACT systems. Garcia-Uribe et al. [97] demonstrated a PACT system using optical fiber bundle for light delivery, as shown in Fig. 3(c). A Q-switched pulsed laser light was coupled to a fused-end, bifurcated fiber bundle that flanked both sides of a commercially available ultrasonic transducer array probe. The fiber optic bundle was encapsulated in a custom enclosure surrounding the transducer array and electronics to provide an easy-to-operate, ergonomic integrated unit. The advantage of this system is the integration of PACT and clinical US (iU22, Philips Healthcare) systems making this system operating for both PA and US imaging. However, the raw channel data of this commercial US system cannot be obtained, and engineers will have to cooperate with Philips to use the specially modified system.

In addition to the three systems mentioned above, many other groups have also invented PAM and PACT systems based on fiber optic light transmission technology for various clinical applications. Table 1 summarizes various PAM and PACT systems by using fiber optic light transmission technologies.

For the OR-PAM system, most groups use the MMF or the fiber bundle instead of the SMF because they can deliver more light energy than the SMF. Moothanchery et al. [98] proposed an OR-PAM system by using an MMF. The MMF was used as the optical excitation source for high resolution OR-PAM in vivo imaging. The use of MMF for achieving tight optical focus would make the optical alignment easier and high repetition rate light delivery possible for highspeed OR-PAM imaging. This system's advantage is that it can achieve a lateral resolution of 3.5 μm, an axial resolution of 27 μm, and an imaging depth of 1.5 mm. This paper also discusses the performance between 10 μm MMF and 25 μm MMF with SMF. However, 10 μm MMF and 25 μm MMF are not commonly used MMFs, and larger MMFs should be studied. Hajireza et al. [99] developed an OR-PAM system by using optical fiber bundle. This fiber bundle with 800 μm image guides consisted of 30,000 individual single-mode fibers. The proposed system kept many of the powerful properties of conventional tabletop OR-PAM systems and presented a submillimeter probe footprint and high flexibility due to the nature of the fiber bundle image-guide. The advantage of this system is that it can be inserted into the body, but at the same time, its scanning range is limited.

For the AR-PAM system, AR illumination requires more light energy than the OR-PAM system, so the MMF is a better choice than the SMF. Baik et al. [100] invented an AR-PAM system based on an MMF. This AR-PAM system integrated Micro MEMS scanner and two linear motor stages featured ultra-wide-field imaging. This system could be used for microvasculature and microstructures imaging. This system's advantage is that it can provide high-speed imaging for wide-field scanning (30 mm × 80 mm). However, the resolution of this system is relatively low.

For the OR/AR-PAM system, some researchers integrate them into one system by using different types of optical fibers. Xing et al. [82] integrated OR-PAM and AR-PAM system together by delivering light via an optical fiber bundle. To achieve a smaller spot size and thus a higher lateral resolution, a single fiber core was used to transmit light for OR illumination, and all the 10,000 fiber cores were used to transmit more energy for AR illumination. This system features automatically higher-resolution OR and deeper AR photoacoustic imaging. However, the imaging speed is relatively slow due to two-dimensional mechanical scanning.

Cai et al. [101] also reported a PAM system consisting of both AR-PAM and OR-PAM based on an SMF and an MMF. This system was used for imaging and characterization of poly (lactic-glycolic acid) polymer scaffolds incorporating single-walled carbon nanotubes (SWNT). For OR-PAM, the light was coupled into an SMF while for AR-PAM the light was coupled into a multimode optical fiber to obtain more energy. This system can be used for noninvasive imaging and monitoring of tissue engineering scaffolds under physiological conditions in vitro and in vivo. The advantage of this system is that it can provide higher-resolution OR and deeper AR photoacoustic imaging. However, it is not simultaneous imaging. Moothanchery et al. [102] developed a high-speed OR-PAM and AR-PAM system by using two multimode fibers. The system was an integrated AR and OR-PAM system equipped with a MEMS scanner and a mechanical stage that could

Table 1
Fiber optic light transmission in PAM and PACT. SMF, single mode fiber; NA, numerical aperture; MMF, multimode fiber; L, Lateral; A, Axial; SWNT, single-walled carbon-nanotube.

Modality	Fiber optics properties	Light source	Ultrasound system	Resolution (μm)	Depth (mm)	Medical Application	Testing sample	Reference
OR-PAM	SMF (NA = 0.28)	532 nm laser	50 MHz, Olympus	L: 12 A: 30	1	Melanoma imaging	Phantom, Mouse	Park [95]
OR-PAM	220 μm MMF (NA = 0.53)	532 nm laser	20 MHz, Olympus	1.5	–	Minimal invasive surgery	Knot	Papado-poulos [96]
OR-PAM	10 μm MMF (NA = 0.10)/ 25 μm MMF	532 nm laser	50 MHz, Olympus	L: 3.5 A: 27	1.5	In vivo imaging	Mouse	Moothanch-ery [98]
OR-PAM	Fiber bundle	532 nm laser	10 MHz, CD International	L: 7	–	Minimal invasive surgery	Mouse	Hajireza [99]
AR-PAM	MMF	532 nm laser	–	L: 84 A: 38	2.3	Microvasculature, microstructures	Mouse, Human palm	Baik [100]
OR/AR-PAM	Fiber bundle	532 nm laser	50 MHz, Olympus	L: 2.2/40	1.3/3	Anatomic imaging	Mouse	Xing [82]
OR/AR-PAM	SMF (NA = 0.13)/ 1000 μm MMF (NA = 0.39)	532 nm laser	50 MHz, Olympus	L: 2.6/45 A: 15	1/3	Noninvasive imaging	SWNT scaffolds in blood or in soft tissue	Cai [101]
OR/AR-PAM	10 μm MMF (NA = 0.10) / 400 μm MMF (NA = 0.39)	532, 586 nm laser	50 MHz, Olympus	L: 5/84 A: 27	0.9/2	Preclinical and skin imaging	Mouse	Moothanch-ery [102]
PACT	Fiber bundle	690–900 nm OPO laser	24 MHz, 128-element, Vermon	L: 84 A: 38	5	Dermatology	Phantom, Mouse, Human skin lesions	Vionnet [75]
PACT	Fiber bundle	532, 665 nm laser	5–12, 4–8 MHz, 128-element, Philips	–	–	Breast cancer detection and treatment	Human breast	Garcia-Uribe [97]
PACT	Fiber bundle	730–830 nm laser	8 MHz, 128-element, Imasonic SaS	100	10	Clinical vascular imaging	Human foot	Taruttis [77]

perform wide-area imaging at high speed. 10 μm core size MMF was applied in OR-PAM system, and 400 μm core size MMF was utilized in AR-PAM system. The system is characterized by high-speed wide-area scanning simultaneous multi-scale photoacoustic microscopy. However, its resolution and imaging depth are lower than other AR/OR-PAM systems.

The PACT system requires deep tissue penetration and wide-area illumination. Compared with SMF and MMF, the fiber bundle is more suitable for use in this type of system. Vionnet [75] et al. proposed a PACT system based on a fiber bundle. The fiber bundle with two linear arms is used to transmit excitation light and guide it to the sample. The fiber bundle arm is placed on both sides of the multi-element linear detector for imaging. This system also integrated a 24 MHz central frequency, 128-element array scanner for application in dermatology. The feature of this system is its ability to image healthy tissues and cancer, but its imaging depth is shallow compared with other PACT systems. Taruttis [77] et al. also reported a PACT system based on a fiber bundle. The fiber bundle was set inside of a custom 8 MHz central frequency, 128-element transducer array. These transducer array elements were arranged on a 135° arc in a row facing inward. Compared with linear arrays, the concave shapes performed better capability for PA image reconstruction. The concave arc also left space for the fiber bundle light pulses to illuminate the skin. The developed system for imaging deep tissues of the human body allows clinical evaluation of major blood vessels and microvasculature. The characteristic of this system is that it has advantages in image reconstruction since it uses concave transducer arrays. However, the system has not been optimized for patient comfort.

2.2. Light transmission in MIPAI

In addition to being widely utilized in PAM and PACT system, fiber optic light transmission technology also applied in almost every case of the MIPAI system. In the MIPAI system, light needs to be transmitted into the body as an internal light source. Optical fibers have high light transmission efficiency and high flexibility so that they are widely used for light carriers in the MIPAI system. The MIPAI system is divided into IPA and PAE. Fig. 4 has shown typically cases for fiber optic light transmission technology used in IPA and PAE.

Due to the use of external light sources, PAM and PACT systems have limited imaging depth. In some clinical applications, deeper tissue target needs to be imaged. The IPA system is utilized fiber optic light transmission technology, transfers the external light sources as an internal light source. This allows deeper tissue targets to be imaged. Thus, the IPA system can be used to guide minimally invasive surgery. It can provide real-time high spatial resolution tissue information.

Bell et al. [103] developed an IPA system based on a 1 mm core size MMF as shown in Fig. 4(a). This IPA system offered interventional guidance in an acoustically challenging environment. An MMF was inserted into the hollow needle core to deliver the laser light. The ultrasound probe was then placed outside the tissue and automatically controlled by a robot. The proposed IPA system was tested separately in fat, muscle, brain, skull, and liver tissue. The advantage of this system is that it combines fiber optic transmission technology with novel robotics technology. In this way, surgeries and procedures can be guided in acoustically challenging environments. The problem with this system is that the internal light source cannot homogeneously illuminate the surrounding tissue, which makes the imaging results inaccurate.

Different from the IPA system, in the PAE system, the ultrasound transducer was customized and set inside the body along with the optical fibers. Wang et al. [44] reported a PAE system based on an MMF as shown in Fig. 4(b) for imaging lipid deposition inside the arterial wall. A 35 MHz ring shape transducer and a 400 μm core MMF were aligned concentrically with the hole of the transducer. A 45-degree rod mirror was applied to reflect the transmitted light and ultrasonic signals. A torque coil was utilized to accommodate the optical fiber and electric wire to provide rotational torque directly to the tip of the probe (2.9 mm diameter). They also developed a scanning system including a customized optical rotary joint with electric slip rings, a rotatory motor, and a linear translation stage. This system is characterized by using a kHz repetition rate Raman laser to achieve a very high imaging speed,

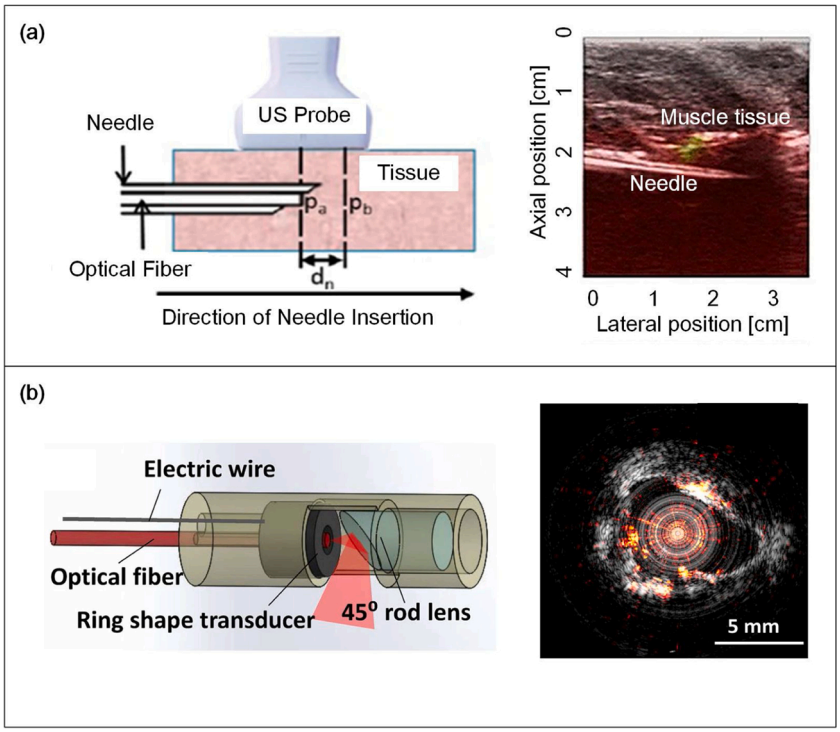

Fig. 4. Embodiments of fiber optic light transmission technology in IPA and PAE. (a) Schematic of the IPA system based on an MMF; IPA image when visualizing the needle tip in muscle. Reprinted and adapted with permission from ref [103]. (b) Schematic of the PAE system based on an MMF; PAE image of the atherosclerotic artery clearly show the complementary information of the artery wall. Reprinted and adapted with permission from ref [44].

reaching 1.0 s per frame. However, its imaging resolution is relatively low.

Besides the above two MIPAI systems, many other IPA and PAE designs based on fiber optic transmission technology have also been proposed. A summary of MIPAI systems utilizing fiber optic transmission technology categorized based on the imaging modalities (IPA and PAE) is provided in Table 2.

For some IPA systems, the MMF is widely used since it can transmit higher optical energy and is relatively compact. Xia et al. [45] developed an IPA system based on a 910 μm core size MMF. The MMF was used for light delivery, which was positioned in a needle cannula. This research was focused on the development and characterization of IPA systems for performing multispectral photoacoustic imaging. Two near-infrared wavelength ranges (750–900 nm and 1150–1300 nm) were applied in the system. These were selected because of the good optical absorption of hemoglobin and lipids. This system provides robust contrast for vasculature and nerves during minimally invasive surgery. The advantage of this system is that its imaging depth is relatively high, but its lateral resolution is relatively low. Lin et al. [64] reported an IPA system utilizing a 2.8 mm core size MMF for in vivo deep brain imaging. By applying internal illumination with an optical fiber in the oral cavity, they showed precise photoacoustic images of the deep rat brain in vivo. Compared to external lighting through the skull, internal lighting provided more light energy to the bottom of the brain. They also applied a 512-element full-ring-shape ultra-sonic transducer array outside of rat brain for PA signal detection. Therefore, their IPA system successfully revealed the deep structures of the brain including the hypothalamus, brain stem, and medulla oblongata. The advantage of this system is that its imaging resolution is relatively high, but its imaging depth is relatively low. Singh et al. [65] proposed an IPA system that used a 600 μm core size MMF for prostate cancer treatment. Their system was employed to image the brachytherapy seeds, which operated in radiation treatment for cancer. Their approach was dedicated to eliminating reflection artifacts caused by the strong signals from the optical fiber and needle tip reflecting off the seed. Their method included several steps. First, the conventional IPA image was detected. The US transducer was then focused at the optical fiber needle tip to get the mimic of the reflected signals. Finally, corrected PA image achieved by subtracting the mimic reflected signals image from the original PA image. Their method provided accurate visualization of the distribution of brachytherapy seeds. This system's advantage is that it can eliminate reflection artifacts caused by the strong signals from the optical fiber. However, its imaging depth is relatively low because they use a relatively small MMF.

For other IPA systems, the fiber bundle can also be used since it could be set around the interventional tool. Francis et al. [68] proposed an IPA system based on a fiber bundle on improving the accuracy of the radiofrequency ablation procedure. Two illumination strategies were applied and characterized in this system, which was divided into extracorporeal and interstitial light delivery. In extracorporeal illumination, the fiber bundle was split into seven sub-bundles with a diameter of 4 mm. In interstitial illumination, a custom-made annular fiber probe with diameter of 3.4 mm was applied. The probe consisted of two steel ferrules with 72 fibers (100 μm, NA = 0.2) arranged between them. The inner ferrule is designed to accommodate interventional needle in its lumen. The experimental results show that the interstitial illumination can assist needle guidance several centimeters inside the tissue. The advantage of this system is that it increases the imaging depth by using a fiber optic bundle to deliver more light energy. However, there are reconstruction artifacts in the PA images.

The IPA system mentioned above mainly relies on light illumination either from the single bare fiber tip or from a fiber bundle, which may not homogeneously illuminate the surrounding tissue. To overcome

Table 2
Fiber optic light transmission in IPA and PAE. SMF, single mode fiber; NA, numerical aperture; MMF, multimode fiber; L, lateral; A, axial; T, transverse; R, radial; UT, ultrasonic transducer; MOPA, master oscillator power amplifier; GRIN, graded index.

Modality	Fiber optics properties	Light source	Ultrasound system	Resolution (μm)	Depth (mm)	Medical application	Testing sample	Reference
IPA	910 μm MMF (NA = 0.22)	700–2200 nm OPO laser	5–12 MHz, SonixMDP	L: 600–1000 A: 100	38	Fetal surgery	Phantom, Human placenta	Xia [45]
IPA	2.8 mm MMF	780 nm laser	5 MHz, ring UT	T: 250 A: 100	16	Deep brain imaging	Mouse brain	Lin [64]
IPA	600 μm MMF (NA = 0.22)	720–860 nm OPO laser	7.5 MHz, Esaote	–	24	Prostate cancer treatment	Phantom, Porcine tissue	Singh [65]
IPA	1 mm MMF	1064 nm laser	5.5 MHz Alpinion	L: 2000 A: 1000	10–30	Interventional guidance	Chicken, Steak Sheep liver	Bell [103]
IPA	Fiber bundle	720–860 nm OPO laser	5.5 MHz Alpinion	–	32	Radiofrequencyablation on liver	Bovine liver tissue	Francis [68]
IPA	1.5 mm MMF with 3 cm long diffuser	1064 nm laser	5 MHz, Verasonics	L: 931 A: 419	75	Cancer screening	Phantom, Mouse	Li [104]
IPA	1 mm MMF 2 cm long diffuser	675–2500 nm OPO laser	5–14 MHz, Analogic	–	35	Prostate imaging	Phantom	Ai [66]
IPA	2 mm MMF 5 cm long diffuser	1064 nm laser	5–9 MHz, Philips	–	70	Prostate imaging	Phantom	Bungart [67]
Modality	Fiber optics properties	Light source	Ultrasound system	Resolution (μm)	Size (mm)	Medical application	Testing sample	Reference
PAE	SMF	527 nm laser	15 MHz unfocused UT	T:49 R:121	9	Gastrointestinal tract imaging	Phantom, Rabbit rectum	Xiong [69]
PAE	SMF	532 nm laser	40 MHz focused UT	L:3.1 A:46.5	20	Vascular network imaging	Human ectocervix	Qu [72]
PAE	365 μm MMF (NA = 0.22)	570 nm laser	43 MHz, unfocused UT	T: 177–520 R: 47–65	4.2	Gastrointestinal tract imaging	Rat tissue samples	Yang [70]
PAE	365 μm MMF (NA = 0.22)	584 nm laser	40 MHz, focused UT	T:100 R:58	2.5	Gastrointestinal tract imaging	Rat colon	Yang [71]
PAE	200 μm MMF	532 nm laser	39 MHz, ring UT	L:230–480 A:34–40	2.3	Intravascular imaging	Phantom, Rabbit aorta	Wei [105]
PAE	400 μm MMF	1064 nm MOPA	35 MHz, ring UT	–	2.9	Intravascular imaging	Miniature pig arterial tissue	Wang [44]
PAE	Six 550 μm MMF (NA = 0.22)	532 nm laser	5–10 MHz, Verasonics	L:300 A:211	7.5	Cervical cancer diagnostic	Phantom	Basija [73]
PAE	GRIN MMF	1030 nm laser	42 MHz, Blatek	L:29.6 A:102	1.4	Intravascular imaging	Femoral artery stent	Zhang [106]

these non-homogeneous problems, many research groups have applied fiber diffusers to their IPA system. Li et al. [104] reported an IPA system with a 1.5 mm core size MMF with a 3 cm long needle-shaped silica diffuser to enable uniform illumination of a large tissue volume. They imaged a 75 mm depth leaf target embedded in optically scattering medium and the mouse heart overlaid with 37 mm thick chicken tissue. This system achieved a deeper imaging depth and larger volume of tissue compared with traditional tip illumination IPA systems. The system could be used for imaging prostate, the bladder, and kidney close to the urethra and ureter, and the lung close to the trachea. The advantage of this system is the high imaging depth. However, the light energy delivered to the target is limited by the fiber damage threshold. Ai et al. [66] developed an IPA system with a 1 mm core size MMF with 2 cm long diffuser. The fiber diffuser was configured to diffuse light from its side surface. The optical fiber was fixed with a 3D-printed plastic mount. A mirror was stuck on the fiber holder to align the fiber with the cylindrical mirror. A 45° reflection surface at the end of the cylindrical mirror reflects the fiber tip light to side direction. The assembled fiber was then inserted into a 25 Fr cystoscope sheath with 8.3 mm diameter. The system was applied for in vivo imaging of prostate cancer. The results indicated that this probe has the has the potential to image the entire prostate by delivering high optical power. The advantage of this system it uses a cylindrical lens array to homogenize the incident beam before a coupling lens thereby reducing the risk of fiber damage. However, its imaging depth is relatively low compared with other IPA system with fiber diffusers. Bungart et al. [67] reported an IPA system based on a 2 mm core size MMF and a fiber diffuser. The fiber diffuser was fabricated by first cleaving and polishing the optical fiber end. The 5 cm length coating and cladding were then removed from the fiber end with a razor blade. The diffuser was fabricated using sandpaper to abrade only the side of the bare fiber end. This design with cylindrical illumination was developed for whole-prostate imaging, and its performance with a phantom was good. Versus Ai et al.'s design [66], the device diameter was reduced from 8.3 mm to 4 mm. This reduces the acoustic shadowing of the anterior prostate. The advantage of this system is that its coupled angle-modulated cylindrical light diffuser provides a relatively high imaging depth. However, in the fabrication process of this fiber diffuser, the use of sandpaper may damage the denuded fibers.

Unlike IPA systems that always use large core optical fibers (>600 μm), PAE systems mainly use small core (<600 μm) optical fibers because of endoscopy size limitations; even single mode fibers are used. Some groups use the SMF in the PAE system. In one example, Xiong et al. [69] built a PAE system with an SMF. One end of the SMF is encapsulated by a custom ceramic ferrule with an outer diameter of 1 mm for light emission. The endoscope was integrated into an aspheric lens and a liquid lens to automatically adjust the optical focal length. A 45° mirror was set in the endoscope for reflecting the light to the target tissue. A customized unfocused 15 MHz ultrasonic transducer was set beneath the mirror. A rotating shaft was applied to the endoscope for 360° field of view. All these components were fixed coaxially in a stainless-steel shell tube. The total diameter of this endo-scope was 9 mm. The PAE system achieved a relatively high resolution of 49 μm and works well for phantom and ex vivo experiments. This system's outstanding feature is autofocusing—traditional systems can only work at a single focal length. This autofocusing can solve problems whereby transverse resolution drops rapidly as the focus moves away from the target boundary. However, its size is a bit larger compared with other PAE probes. Qu et al. [72] also developed a PAE system based on an SMF. This probe applied a set of doublets and a 40 MHz custom-designed focused ultrasonic ring transducer. These parts were set to coaxial confocal alignment. A MEMS scanning mirror derived focus scanning parallel to the cylindrical axis of the probe. This PAE system could achieve a 250 Hz B-scan rate over a 3-mm scanning range. In comparison, the B-scan rate of a typical PAE system was 10 Hz. This PAE system was used to identify the differences in vascular morphology be-tween human cervix as well as the differences in longitudinal and cross-sectional areas of the cervical vasculature of pregnant women. This system was also used to screen for visceral pathological changes related to angiogenesis. This system is fast scanning, but the probe is too big.

In addition to applying the SMF in PAE systems, most PAE systems use relatively small core (<600 μm) multi-mode fibers to deliver light. Yang et al. [70] reported a PAE system based on a 365 μm core size MMF. This endoscope consisted of an MMF, a single-element ultrasonic transducer, a scanning mirror, and a mechanical micromotor. The scanning mirror was placed 45° to the endoscope 's axis, driven by the micromotor for 360° field of view. All these components were placed into a stainless-steel tube. The endoscope diameter was 4.2 mm, which could be complementary to other forms of endoscopy since it is able to reach depths beyond the optical transport mean free path. The feature of this system is that it is the first small PAE system proposed at that time. However, the full ring-views cannot be achieved due to the stainless-steel wall restriction. Yang et al. [71] then improved their first generation PAE system by reducing the diameter from 4.2 mm to 2.5 mm. To achieve sufficient signal sensitivity in this size, they designed a novel lead magnesium niobite lead titanate (PMN-PT) focused US transducer. This mini probe could be inserted into a standard video endoscope to guide the video endoscope. Moreover, this PAE system could work as endoscopic ultrasound system for simultaneous PAE and EUS imaging for complementary contrast. This has a small diameter, but its length is relatively long (35 mm), and the long probe cannot be bent, which may be limited in some medical applications. Wei et al. [105] presented a PAE system using a 200 μm core size MMF. This system integrated a miniaturized probe combining US and PA. The PAE system consisted of an MMF, a 39 MHz ring-shaped US transducer, and a micromirror. In contrast to other PAE systems, this system did not include the micromotor in the probe, and the probe diameter was only 2.3 mm. For circumferential scanning (B-scan), the test sample was fixed in a water tank driven by a stepping motor. The coaxially designed probe provided accurate IVUS and IVPA images of normal rabbit aorta. The advantage of this system is its small diameter, but the probe cannot rotate autonomously. Basija et al. [73] reported a PAE system with six 550-μm core multimode fibers. This system also could work in US and PA mode. A 64-element ultrasound phased-array transducer was coupled to a fiber-optic light delivery system (6 multimode fibers) for PA and US imaging. The system also did not include the micromotor inside the probe, so that for the phantom test, the testing stage was rotated by stepper motors. The diameter of the probe was 7.5 mm. The main application was the visualization and detection of early-stage gynecological malignancies. The test results show that the system can identify carcinogenic tissue in the cervical canal and other hard-to-reach clinical diagnosis areas. The advantage of this system is its phased-array ultrasound and photoacoustic imaging capabilities. However, this probe also cannot rotate autonomously. Zhang et al. [106] designed a 1.4 mm diameter PAE system with a graded index multimode fiber (GRIN MMF). The GRIN MMF featured high beam quality based on beam self-cleaning effect. Therefore, this probe could keep the clean mode for a high-energy pulse. The resulting fluence reached 20 μJ, which is two orders of magnitude higher than a PAE system built with a SMF. This probe consisted a GRIN MMF, a GRIN lens, a prism, and an ultrasound transducer. A motor was installed outside the probe and connected to the optical fiber to rotate the probe. The advantages of this system are small size, high resolution, and high pulse energy. However, this system is not robust for high-speed rotation.

In conclusion, fiber optic light transmission technology is widely used in different modalities of photoacoustic imaging. It is an essential part of many compact and convenient photoacoustic imaging system.

3. Fiber optic US transmission

Fiber optic technology has been used not only to transmit light but also to transmit US for PAI in recent years. In standard PAI, endogenous/

exogenous contrast agents are on the target sample. However, in this fiber optic US transmission structure, the contrast agents are directly coated on optical fibers, as shown in Fig. 5, so the optical fibers can generate and transmit US signals. This fiber optic US system can generate broadband wide-angle US signals and can provide complementary image contrast as standard PAI. It can also be recognized as an US imaging based on the principle of PA effect.

The principle for fiber optic US transmission system is that US signals are generated and transmitted by illuminating the composites on optics fibers. Compared with conventional technologies, the fiber optic US transmission technology has the following advantages: 1) The transducer is compact. The outer diameter of one sensor is approximately hundreds of micrometers. 2) The transducer features a wide bandwidth that will provide high image resolution. 3) The transducer is easy to manufacture and low cost. 4) There is no electromagnetic interference for fiber optic US transmission element. 5) Some fiber optic US transmitters can transmit US signals at multiple points along a single fiber. Table 3 summarizes various fiber optic US transmission systems. These systems are mainly used in intravascular imaging, which can be categorized as IPA or PA based ultrasound imaging.

Most fiber optic US transmission systems have the contrast agent dip coated on the optical fiber tip. Colchester et al. [107] proposed a fiber optic US transmission probe shown in Fig. 5. Carbon nanotube (CNT)–polydimethylsiloxane (PDMS) was used as the contrast agents. The multi-walled carbon nanotubes were functionalized and dissolved in xylene. Fig. 5(a) shows the chemical process of its synthesis. The CNT-PDMS composite solution was manufactured by manually mixing functionalized CNT/xylene solution with PDMS. This was followed by sonicating and degassing. A CNT-PDMS composite was dip coated on the tip of two MMFs with diameters of 105 and 200 μm. The US pressures and bandwidths of these fiber optic probes were measured and were consistent with values used for intravascular imaging. The feature of this system is the synthesis of CNT-PDMS composite material for the contrast agent. However, the biomedical application of the system needs to be verified by some animal or phantom tests. Zou et al. [108] developed a fiber optic US transmission probe whereby gold nanoparticles (AuNPs) within PDMS were ap-plied in the system. The materials synthesis followed a one-pot protocol by directly mixing the gold salt ($HAuCl_4 \cdot 3H_2O$) into PDMS. After sonicating and degassing, AuNPs-PDMS composite was dip coating on the tip of a 400 μm core size MMF. The ultrasound profile and the acoustic distribution had been characterized. They also demonstrated its capability for C mode US imaging of a tissue specimen. This system is characterized by the synthesis of AuNPs-PDMS composite for the contrast agent. However, the imaging speed is relatively slow. Poduval et al. [109] presented a fiber optic US transmission probe based on multiwall carbon nanotube (MWCNT)-polyvinyl alcohol (PVA)-PDMS material. The MWCNT in PVA was directly electrospun onto a 200-μm core size MMF and subsequently dip-coated with PDMS. The electrospun probe generated ultrasonic pressures in the MPa range at a low pulse energy of 11 μJ, which is suitable for clinical use. This system is characterized by the synthesis of MWCNT-PVA-PDMS composite for the contrast agent. However, the verification of the system lacks some animal or phantom tests. Vannacci et al. [110] described a fiber optic US probe using a new Micro-Opto-Mechanical System (MOMS) for endoscopic tissue analysis. Carbon films were used as contrast agents and were fabricated on miniaturized single-crystal silicon frames used to mount the probe on the tip of optical fibers. A polymer FP layer was also integrated for the detection function. The proposed system could be used in biomedical applications of broadband ultrasound through miniaturized fiber optic devices. This system is characterized by the synthesis carbon films for the contrast agent but still requires phantom and in vivo validation. Chang et al. [111]

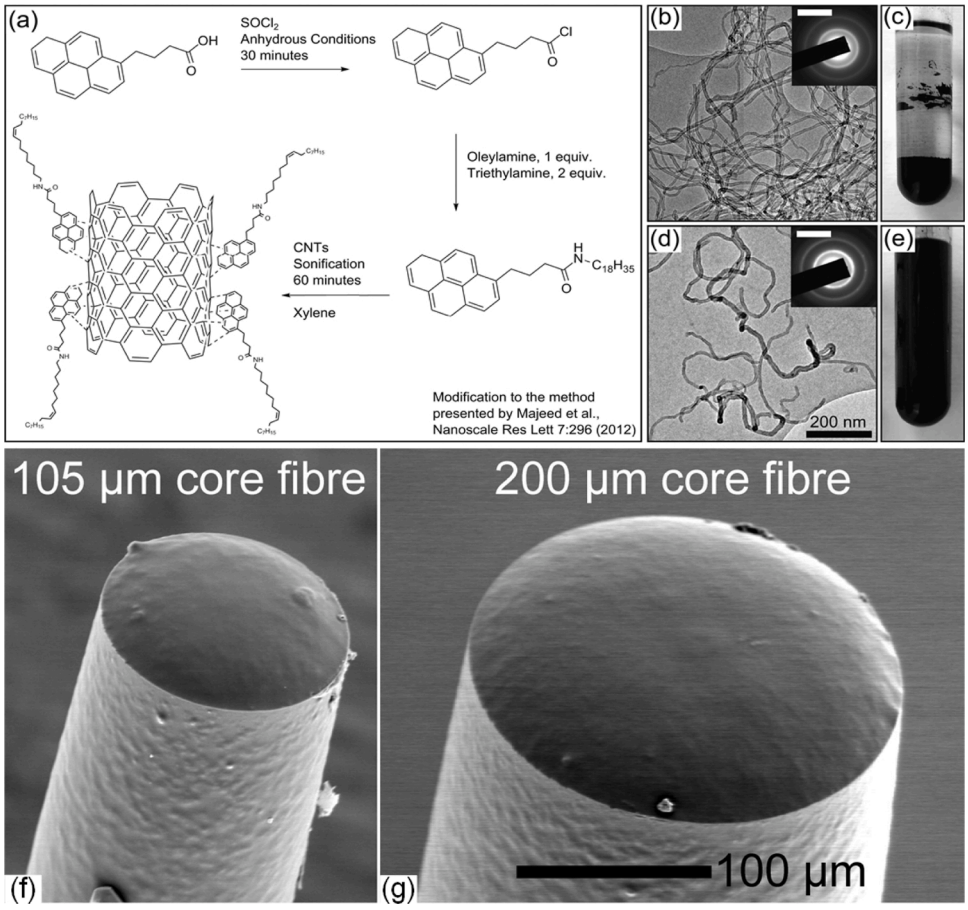

Fig. 5. Embodiments of fiber optic US transmission probe. (a) Schematic of the chemical process to functionalize multi-walled carbon nanotubes (CNTs) in xylene. (b) Transmission electron microscopy (TEM) image of non-functionalized CNTs, with inset showing corresponding selected area electron diffraction (SAED) pattern indicating carbon (scale bar: 5 nm^{-1}). (c) Non-functionalized CNTs in xylene. (d) TEM image of functionalized CNTs, with inset showing corresponding SAED indicating carbon (scale bar 5 nm^{-1}). (e) Functionalized CNTs in xylene. (F-g) Optical fibers after dip coating with the CNT-PDMS composite on 105 and 200 μm optical fiber. Reprinted and adapted with permission from ref [107].

Table 3
Fiber optic US transmission in PAI. SMF, single mode fiber; MMF, multimode fiber; CNT, carbon nanotube; PDMS, Polydimethylsiloxane; AuNP, gold nanoparticles; MWCNT, multiwall carbon nanotube; PVA, polyvinyl alcohol; CSNPs, candle soot nanoparticles; FP, Fabry-Perot; rGO, reduced graphene oxide; CB, carbon black; A, axial.

Modality	Fiber optics properties	Contrast agents	Light source	Ultrasound system	Resolution (μm)	Medical application	Testing sample	Reference
IPA	105, 200 μm MMF	CNT - PDMS	1064 nm laser	30 MHz Precision Acoustics	–	Miniature US imaging	–	Colchester [107]
IPA	400 μm MMF (NA = 0.39)	AuNP - PDMS	532 nm laser	40MHz, Onda	200	Intravascular imaging	Pork tissue	Zou [108]
IPA	200 μm MMF (NA = 0.22)	MWCNT - PVA -PDMS	1064 nm laser	30 MHz Precision Acoustics	–	Minimally invasive surgery	–	Poduval [109]
IPA	200, 600 μm MMF	Carbon films	1064 nm laser	40MHz, Onda	–	Minimally invasive surgery	–	Vannacci [110]
IPA	–	CSNPs-PDMS	532 nmlaser	40MHz, Onda	–	Ultrasound therapy	–	Chang [111]
IPA	600 μm MMF	rGO-PDMS	1064 nm laser	30 MHz Precision Acoustics	–	Minimally invasive surgery	–	Colchester [112]
IPA	Four 105 μm MMFs (NA = 0.22)	AuNP - PDMS	532 nm laser	40MHz, Onda	200	Intravascular imaging	–	Zhou [113]
IPA	600 μm MMF (NA = 0.39)	AuNP - PDMS	532 nm laser	40MHz, Onda	–	Intravascular imaging	–	Zhou [114]
IPA	Two SMFs with one coreless fiber 200, 600 μm	Graphite –epoxy resin	1550 nm laser with EDFA	7.5 MHz, Olympus	–	Miniature imaging	–	Li [115]
PAE	MMF (NA = 0.39)	CNT-PDMS	1064 nm laser	30 MHz Precision Acoustics, FP sensor	–	Interventional applications	Swine aorta	Alles [116]
PAE	200 μm MMF (NA = 0.22)	CNT-PDMS	1064 nm laser	20 MHz, FP sensor	L: 88 A: 64	Intravascular imaging	Swine carotid artery	Colchester [117]
PAE	200 μm MMF	MWCNT-PDMS	1064 nm laser	60 MHz Precision Acoustics, FP sensor	–	Intravascular imaging	Swine aorta	Noimark [53]
PAE	105, 200, 400 μm MMF	PDMS composites	532 nm laser	FP sensor	–	Intravascular imaging	Human placenta, Ex vivo human tissue, Pork belly	Noimark [118]
PAE	100 μm MMF	CB-PDMS	532 nm laser	40 MHz Onda, FP sensor	A: 31−67 L: 64−112	Endoscopic, intravascular imaging	Phantom	Li [119]
PAE	400 μm MMF	MWCNT-PDMS	1064 nm laser	FP sensor	A: 54−71	Minimally invasive surgery	Swine carotid	Colchester [120]
PAE	1000 μm MMF (N = 0.22)	Thin film	532 nm laser	80 MHz, Force Tech, FP sensor	A: 125	Multimodality imaging	Cyst Phantom	Hsieh [121]
IPA	105, 200 μm MMF	CNT-PDMS	1064 nm laser	5−14 MHz, SonixMDP FP sensor	A: 70	Minimally invasive surgery	Phantom	Xia [122]

reported an ultrasound probe using cCandle soot nanoparticles-polydimethylsiloxane composites (CSNPs-PDMS) as contrast agents. It was confirmed that tThis material could provide efficient light absorption and heat transfer performance. The CSNPs-PDMS composite US transducer showed a high energy conversion coefficient at a broad frequency range among the transducers using the CB-, CNFs-, and CSNPs-PDMS composites. This system is characterized by the synthesis CSNPs-PDMS composite for the contrast agent but still requires further validation. Colchester et al. [112] built a directional fiber optic US probe based on a reduced graphene oxide (rGO)-PDMS composite. Compared with CNT, rGO will not suffer from certain health problems due to the elongated shape of carbon. A 600 μm core size MMF was used for ultrasound generation. The divergence of the US beam was very low, with a distance between 0 and 16 mm. It was very suitable for high-resolution interventional imaging. This system requires synthesis (rGO)-PDMS composite for the contrast agent. However, the biomedical application of the system needs to be verified by some animal or phantom tests.

Some novel fiber optic transmission systems have more than one ultrasonic transmission element. Zhou et al. [113] introduced a fiber optic US phased array transmission system based on four 105 core size MMFs. The AuNPs-PDMS composite was used as contrast agents coated on the tip of four MMFs. Four optical fibers with different lengths could introduce the time delay for each transmitter. A phased array US was built by controlling the length of each optical fiber probe. This system can steer and focus the US signals for clinical intravascular imaging. One feature of this system is the phased array structure.

In addition to the fiber optic tip phased array structure, some researchers built multipoint US generation systems on the sidewall of the optical fiber rather than on the tip of the optical fiber. Zhou et al. [114] built a fiber optic US system, in which the US signals were generated on the sidewall rather than on the tip of the optical fiber. A 600-μm core size MMF and a same AuNPs-PDMS composite were used in this system. The sidewall coating and cladding of the optical fiber were re-moved so that the US can be generated through the sidewall of the fiber. The length of the sidewall emission area could set as 5 mm, 10 mm, 20 mm etc. The benefit of this structure is that multiple US generation elements can be achieved in one single optical fiber. Li et al. [115] also demonstrated a multipoint fiber optic US system using two SMFs with one coreless fiber. The coreless fiber segment's fusion with single-mode fibers were at each end. The length of the coreless fiber was set as 90 μm. Graphite-epoxy resin composite was used as contrast agents. The laser light can emit at the coreless area to contrast agents to generate and transmit the US signals. The feature of this system is the multipoint US generation structure.

In some systems, fiber optic US transmission technology is combined with fiber optic US detection technology (fiber optic FP technology) for all-optical US imaging [53,116–122].

Alles et al. [116] built a pencil beam all-optical US imaging system. CNT-PDMS was used as contrast agents. It was an ultrasound probe that used the transmitted beam's geometric focusing, forming image lines without image reconstruction. It was employed for ex vivo swine aorta imaging (3D). The advantage of this system is its miniature directional all-optical US imaging. However, the lateral resolution of this system is relatively lower than non-directional probes. Colchester et al. [117] introduced an all-optical US probe for high resolution vascular tissue imaging. A 200 μm core size MMF was used for US transmission. CNT-PDMS was used as contrast agents. Ultrasound was detected with an FP cavity on the end face of an adjacent optical fiber. The FP sensor of this system will be discussed in detail in Section 4. The probe was moved across the sample to build a virtual linear array of ultrasound transmit/receive elements. It was applied for the ex vivo swine carotid and aorta imaging (2D). The advantage of this system is its high-resolution imaging. The lack of septum between the US transmitter and receiver may cause crosstalk. Noimark et al. [53] worked on an MWCNT-PDMS material for fiber optics US imaging. A 200 μm core size MMF was used for ultrasound generation. In this work, they mainly discussed the methods for fabricating PDMS and MWCNTs composite coatings. These methods included the use of two solvents to create an MWCNT organogel, dip coating the organogel, and subsequent overcoating with PDMS. These methods allowed the creation of thin and uniform CNT composites on miniature or temperature-sensitive surfaces to achieve a wide range of advanced sensing functions. They also presented an all-optical pulse-echo ultrasound imaging system using an FP sensor as a signal receiver. It was used for the ex vivo swine aorta imaging (2D). This system's advantage is that its ultrasound transmitter achieved strong ultrasound pressures for large tissue penetration depths and wide bandwidths for high-resolution imaging. However, the performance of the FP sensor part of the system has not been discussed in detail. Colchester et al. [120] presented an all-optical rotational B-mode pulse-echo US imaging system. MWCNT-PDMS was used as the contrast agents. A 400 μm MMF was used for US generation element. A concave FP cavity at the distal end of a SMF was used for US detection element. This system demonstrated that it is viable for clinical rotational US imaging. Ex vivo swine carotid imaging (rotational 2D) was applied in this system to investigate the capabilities of the probe. This system is characterized by its all-optical rotating B-mode pulse-echo ultrasound imaging. This system is currently only applied for 2D imaging. It would be better if it could be applied to 3D imaging in the future.

In other systems, fiber optic US transmission technology is not only combined with fiber optic US detection technology, but also combined with fiber optic light transmission technology. These systems perform light delivery for PA imaging and US imaging (i.e. light and US delivery) in a single device, such as Noimark et al. [118], Li et al. [119], Hsieh et al. [121], and Xia et al. [122]. These systems combine high-quality acoustic resolution with high optical contrast.

Noimark et al. [118] also discussed multiple PDMS composites for optical US generation and PA imaging. They reviewed and classified the methods used to create these PDMS composites. By combining different fabrication methods, their approach established next-generation fiber optics US generators. Their imaging examples included ex vivo human placenta imaging (3D) and ex vivo human aorta and pork belly imaging US/PA (2D). The feature of this work is it discusses "all-in-one," "bottom-up," and "top-down" fabrication methods to accelerate the development of the next generation of fiber optic US generators. Li et al. [119] designed a miniature all-optical probe for PA and US imaging. Several optical fibers were used in this system. Two MMFs were used for optical transmission and US transmission. A SMF was used for FP sensor. The FP sensor part of this system will be discussed in Section 4. This system was used for resolution phantom imaging (2D). This system's feature is it combines PA excitation, US generation, and US detection into one single probe. However, this probe requires a protective sheath, which adds bulk. Hsieh et al. [121] developed an all-optical scanhead for both PA and US imaging. A thin film plate was used for US generation. A 1000 μm MMF was used to deliver laser energy. The spot size related with a width of ultrasonic transmit element is 600 μm which was the same as the core size of the optical fiber for optical excitation. A FP structure was used for both the PA and US signal receiver. Cyst phantom imaging (2D) demonstrated this design's feasibility. This system is characterized by US/PA imaging with an all-optical scanning head design. However, the axial resolution of this system is lower than other group designs. Xia et al. [122] designed a PAI system including a fiber optic light transmission PA probe, a fiber optic US transmission probe, and a fiber optic US detection probe (FP sensor). Two MMFs were used for transmission: One part was used to deliver the light and one was used to transmit US. CNT-PDMS was used as the contrast agents coated on the US transmission probe. One SMF was used for US detection. The FP sensor of this system will be discussed in detail in Section 4. This system is characterized by its high-resolution all-optical US/PA imaging. However, these three probes may cause crosstalk because there is no septum between them.

In summary, fiber optic US transmission technology based on the PA effect is becoming increasing common because it offers complementary contrast with standard PAI in minimally invasive imaging.

4. Fiber optic US detection

Fiber optic US detection technology is another major fiber optic technology applied in PAI. This method is to replace the traditional electrical US transducers with fiber optic US receivers. The fiber optic US detection elements are small with relatively high resolution and easy fabrication compared to the electrical detection elements. The most common is fiber optic Fabry-Perot (FP) technology. Other categories of fiber optic US detection technologies include fiber Bragg grating (FBG), micro-ring resonator technology, and fiber laser technology.

4.1. Fiber optic Fabry-Perot technology

Fiber optic Fabry-Perot (FP) technology is based on the FP interferometer. In optics, a FP interferometer is typically made of a transparent plate with two parallel highly reflecting surfaces (i.e.: thin mirrors). These two surfaces forming the FP cavity. The incident light strikes the first surface and some of the light reflects and the rest light continues to propagate until it reaches the second surface. The reflected light from the second surface interferes with the reflected light from the first surface, generating an interference pattern. The interference fringes will be shifted when the FP cavity length changes. Then the shift of the interference fringes can be determined by a photodetector that is monitoring light intensity reflected from the cavity as the cavity length changes. By monitoring the light intensity changes, the US signal can be detected. Typically, the fiber optic FP probe consists of two reflective mirrors and a polymer layer in between to form an FP interferometer (Fig. 6).

Ansari et al. [123] developed a PAE system based on the fiber optic light transmission technology and the fiber optic FP technology. This is an all-optical forward-viewing PAE probe for high-resolution 3D imaging. An optical fiber bundle with a diameter of 3.2 mm was used to transmit light and detect the US signals through its end-face FP interferometer structure. The FP structure was made by two dielectric mirror coatings sandwiched between a Parylene C spacer layer (Fig. 6). The fiber bundle contained 50,000 individual elements—each with a diameter of 12 μm. These serve as individually US receivers. The end of the fiber bundle was polished to form an 8-degree angle to reduce interference caused by each element. 3D images of phantoms, duck embryos, and mouse skin were detected by this all-optical forward-viewing PAE system. Photoacoustic image of an ex vivo duck embryo is shown in Fig. 6 (e–j). This system has an all-optical front-viewing endoscopic probe and a larger size versus other PAE probes.

Researchers have presented various types of fiber optic FP systems (Table 4). In transmission mode, some systems use fiber optic light transmission technology, some use fiber optic US transmission

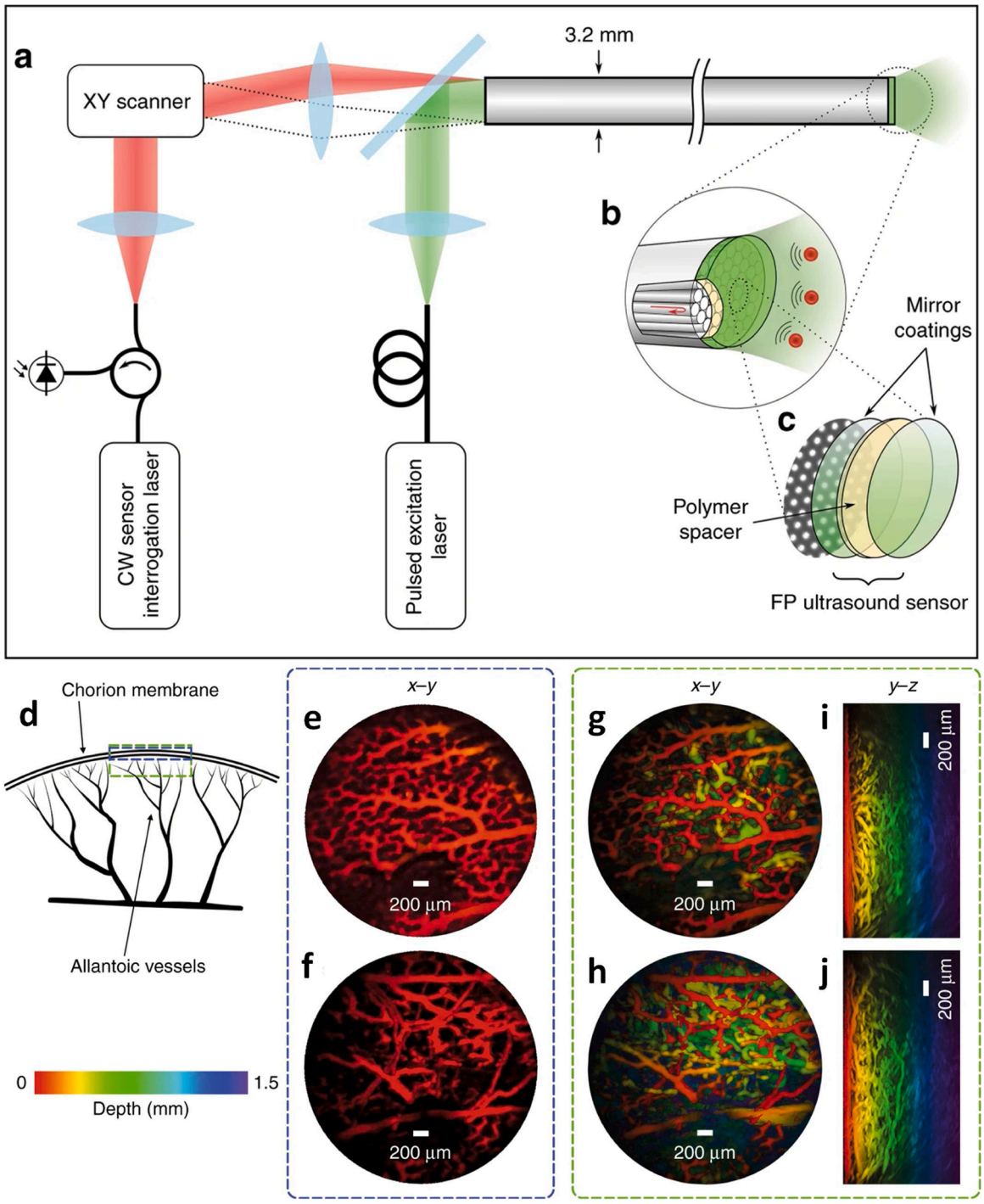

Fig. 6. Embodiments of a fiber optic FP system. (a) A schematic representation of an all-optical forward-viewing photoacoustic endoscopy probe. (b) A magnified visualization of the fiber end. (c) A structure of the FP sensor. (d) A schematic diagram of an avian embryonic vasculature. (e, f) x–y maximum intensity projections for a microvascular anatomy of the chorioallantoic membrane, in two regions of the same embryo [z = 0-200 µm]. (g, h) x–y maximum intensity projections for the same two regions as in e and f [z = 0-1.5 mm]. (i, j) y–z maximum intensity projections for the same two regions. Reprinted and adapted with permission from ref [123].

technology, and others combine these two technologies.

Several groups have combined fiber optic light transmission technology with fiber optic FP technology. Zhang et al. [81] proposed a PAE system using a dual cladding optical fiber. This optical fiber combines both single-mode and multimode characteristics. The FP structure was built by a polymer spacer sandwiched between a pair of dichroic dielectric mirrors. The probe diameter was only 0.25 mm. The PAE probe was also designed with two structures: front view and side view. The acoustic bandwidth and sensitivity of the probe were evaluated. The FP probe achieved ultra-high acoustic sensitivity. This all-optical design of the PAE system can benefit a variety of endoscopic applications. This system is miniatured but has yet to validated in vivo. Miida et al. [124] reported a PAE system consisting of a fiber optic FP probe for ultrasound detection and a bundle of hollow optical fibers for light excitation. A thin polymer film was attached to the SMF tip for generating the FP structure. In theory, the FP sensitivity of this structure should be lower than the FP

Table 4
Fiber optic FP technology in PAI. NEP, noise equivalent pressure; SMF, single mode fiber; MMF, multimode fiber; L, lateral; A, axial; CNT, carbon nanotube; PDMS, Polydimethylsiloxane; AuNP, gold nanoparticles; MWCNT, multiwall carbon nanotube; CB, carbon black.

Modality	Fiber optics properties	Contrast agents	Light source	FP structure	Resolution (μm)	Size (mm)	Medical application	Testing sample	Band width (MHz)	Sensitivity	Reference
PAE	Dual cladding optical fiber	–	1064 nm laser	Dichroic coatings /Polymer	–	0.25	Intra-vascular imaging	Phantom	20	NEP:8 Pa	Zhang [81]
PAE	3.2 mm fiber bundle: PA SMF: FP	–	532 nm laser	Thin polymer film	L: 500 A: 250	–	Endoscope and catheter imaging	Phantom	10	–	Miida [124]
PAE	3.2 mm fiber bundle	–	1064 nm laser	Dielectric coatings /Parylene C	L: 45–170 A: 31	3.2	Fetal surgery	Duck embryo, Mouse skin	45	–	Ansari [123]
PAE	200 μm (NA = 0.22) MMF: US SMF: FP	CNT-PDMS	1064 nm laser	Dielectric coatings /Epoxy	L: 88 A: 64	0.84	Intra-vascular imaging	Swine carotid artery	20	–	Colchester [117]
PAE	300 μm (NA = 0.22) MMF: US SMF: FP	MWCNT -PDMS	1064 nm laser	Dielectric coatings /polymer	A: 64	1.08	Minimally invasive surgery	Swine heart	26.5	–	Finlay [125]
PAE	3.15 mm fiber bundle SMF: FP	CB - spray paint	532 nm laser	Dielectric coatings /Parylene C	X: 97 Y: 179 Z: 110	3.5	Endoscopic imaging	Porcine cardiac tissue	27	–	Alles [126]
PAE	1 mm MMF: US (NA = 0.39) SMF: FP	AuNP-PDMS	532 nm laser	Gold coatings /PDMS	–	–	Intra-vascular imaging	Pork tissue	20	–	Zhou [127]
PAE	105, 200, 400 μm MMF	PDMS composites	532 nm laser	Gold coatings /Parylene C	A: 64	1.08	Intra-vascular imaging	Human placenta, Ex vivo human tissue, Pork belly	26.5	–	Noimark [118]
PAE	200 μm (NA: 0.5) MMF: PA 100 μm MMF: US SMF: FP	CB-PDMS	532 nm laser	Gold coatings /Parylene C	A: 72–117 L: 104–154 A: 31–67 L: 64–112	2	Endo-scopic and Intra-vascular imaging	Phantom	29	NEP: 0.4 KPa	Li [119]
PAE	1000 μm (N = 0.22) MMF: PA 600 μm MMF: US SMF: FP	Thin film	532 nm laser	Polymer microring resonator	A: 125	–	Multi-modality imaging	Cyst Phantom	22.6	–	Hsieh [121]
PAE	105, 200 μm MMF: PA, US SMF: FP	CNT - PDMS	1064 nm laser	Dielectric coatings /Parylene C	A: 70	–	Minimally invasive surgery	Phantom	–	–	Xia [122]

sensitivity of that sandwich structure. The 3D PA image could be performed by subsequently exciting the hollow fiber at the input end of the fiber bundle, without any mechanical scanning mechanism. Since the NA of the hollow fiber was extremely small, the PA image resolution was the same diameter as the hollow fiber. A 3D PA image of the blood vessel phantom was reconstructed by this PAE system. This all-optical PAE probe without scanning mechanism could be widely used in different medical applications. The system offers an all-optical photoacoustic probe without a scanning mechanism at the distal end but with relatively low resolution.

Several groups have also combined fiber optic US transmission technology with fiber optic FP technology. Colchester et al. [117] introduced an all-optical fiber PAE system for high resolution vascular tissue imaging. The US transmission part of this system has been discussed in Section 3. The FP probe comprised an epoxy spacer sandwiched between two dielectric mirror coatings. The probe had a diameter of less than 0.84 mm and could be used for intravascular imaging. This system offers high-resolution imaging capability, but there is no septum between the US transmitter and receiver, which may cause crosstalk.

Finlay et al. [125] built an PAE system based on a 300 μm core size MMF and an SMF, which the MMF was used for US transmission and the SMF for FP. MWCNT-PDMS composite coating on the tip of MMF for US transmission. Two dielectric mirrors were deposited before and after dip-coating the polymer to form the FP structure. A metallic septum was applied to isolate the two optical fibers. All these parts were set in a custom inner transseptal needle. This system can provide exquisite visualizations of tissue for minimally invasive procedures. The advantage of this system is the robust probe design. However, it would be better if the system can also be applied to 3D imaging. Alles et al. [126] designed a reconfigurable all-optical transducer array for 3D endoscopic imaging. A fiber bundle was for US transmission, and an SMF was for FP. Carbon Black Professional Spray Paint was coated on the distal end-face of the fiber bundle for the US generation. Two dielectric mirror coatings with Parylene C was used to build the FP interferometer structure. A two-axis galvo-mirror and lens were used to focus and steer the laser light arbitrarily to different part of the proximal end of the optical fiber bundle. The optical fiber bundle then transmitted the steered light to the corresponding area of its distal end-face contrast agents for US generation and transmission. Therefore, a US transducer array was built, and it can

be optically reconfigured to optimize system performance. This system completed 3D imaging of phantoms and ex vivo tissues. This system can be applied in various imaging scenarios. The advantage of this system is its ultrasound transducer array for 3D endoscopic imaging but at the expense of larger probe size. Zhou et al. [127] proposed an all-optical fiber imaging system for intravascular imaging. A 1 mm core size MMF was used for US transmission and an SMF was used for FP. AuNP-PDMS was used for contrast agents. Two gold mirror coatings with PDMS was used to build the FP structure. This system accomplished C-mode US imaging of pork tissues and could be used in future intravascular imaging. The advantage of this system is all-optical C-mode US imaging but is relatively delicate and needs a protective sheath.

Other groups combined all these three types of fiber optic technologies in one system [118,119,121,122]. The transmission part of these systems has been discussed in Section 3.

Noimark et al. [118] presented an all-optical system applying three types of fiber technology. They used the same FP probe as Finlay et al. [125]. The system performance is similar to them. Li et al. [119] has also developed a PAE system that uses three types of fiber technology. Two gold mirror coatings with Parylene C was for FP structure. This system combines PA excitation, US generation, and US detection into one single probe. Hsieh et al. [121] developed an all-optical scanhead for both PA and US imaging. Polymer microring resonator was used for the FP sensor. This system is characterized by US/PA imaging with an all-optical scanning head design. However, the axial resolution of this system is lower than other group designs. Xia et al. [122] also presented a PAE system with three optical fibers: one MMF was used for light transmission, one MMF was for US transmission, the other SMF was for US detection (FP probe). Two dielectric mirror coatings with Parylene C was applied on the tip of one MMF to form the FP structure. This system has a high-resolution all-optical US/PA imaging but these three probes may cause crosstalk because there is no septum between them.

4.2. Fiber Bragg Grating technology, Fiber optic Micro-Ring Resonator technology, Fiber laser technology

Other categories of fiber optic US detection technologies have also been designed in recent years for PAI. Some researchers used FBG technology as a US detection method. FBG is another primary technology of fiber optic US detection technology. FBG is made by exposing the core of single-mode fiber to a periodic pattern of intense laser light laterally. Exposure increases the refractive index of the fiber core. FBG could be considered as a combination of many FP cavities. FBG can be used as a US detector, similar to the principle of FP.

Shnaiderman et al. [129] used a fiber optic US detector based on π-phase-shifted FBG for a PAM system. The π-FBG was a special FBG whose spectrum consisted of a narrow resonance fringe and a stop band centered on the fringe. They added this miniaturized photoacoustic US detector to the optical microscope to supplement fluorescence contrast with label-free measurements of light absorption and enhance biological observation. This π-FBG based fiber optic US detector could be integrated into any conventional optical microscope. This hybrid optical and photoacoustic microscope successfully imaged the abdomen and ears of mice. Their technology simplified the integration of sound detection in standard microscopes and made the PAM more accessible to bio-medical imaging. The system is characterized by its miniaturization and can be integrated into any traditional optical microscope. However, for the OR-PAM system, the resolution and imaging depth of the system is relatively low.

Some researchers used MRR technology as a US detection method. Li et al. [130] applied a US detector based on an optical micro-ring resonator for PAM. Compared with the traditional large-size opaque piezoelectric ultrasonic detector, the total thickness of this fiber optic transparent US detector was only 250 μm. It enabled highly-sensitive US detection over a wide receiving angle with a bandwidth of 140 MHz. The estimated noise-equivalent pressure (NEP) was 6.8 Pa. This novel US detector may lead to increased applications for PAM for cancer research, neuroscience, and ophthalmology. This system is characterized by highly-sensitive ultrasound detection over a wide receiving angle, which is favorable for increasing the field-of-view in laser-scanning PAM systems. However, this system has not been commercialized for others to use.

Other researchers used fiber laser technology as a US detection method. Liang et al. [128] applied a small-sized optical fiber based laser for a PAM system. US waves apply pressures on the optical fiber laser caused harmonic vibrations of the fiber, which could be detected by the frequency shift of the fiber laser. The fiber laser was made by applying two wavelengths matched fiber Bragg gratings (FBGs) in series in an optical fiber. An FBG was a type of distributed Bragg reflector constructed in a short segment of optical fiber that reflected particular wavelengths of light and transmits all others. When the US hit the fiber laser, the FBG would cause a frequency shift that could be detected by a photodetector. The fiber laser US detector is thus an important new tool for all-optical photoacoustic imaging. The system offers high resolution and large field-of-view but has limited imaging speed. Liang et al. [94] then utilized an unfocused side-looking fiber optic US detector for a PAM system. This fiber optic US detector was developed based on dual polarization fiber laser and read out by real-time frequency demodulation. This system could be used for imaging physiologic dynamics in both trunk vessels and capillaries. This system is characterized by fast-scanning, high detection sensitivity, high stability, and a large field of view. However, this ultrasonic sensor may suffer some noise interference. Allen et al. [131] designed two types of fiber lasers for PAM and PACT. One was designed for widefield PACT and used custom-drawn optical fiber to provide high pulse energy. Another was designed for OR-PAM and provides a high-quality beam (M^2<1.1) with a pulse repetition frequency (PRF) up to 2 MHz. The compact size (<100 μm) and enhanced functionality of these lasers provided important opportunities to facilitate the transformation of photoacoustic imaging into practical applications in medicine and biology. This system is characterized by its compact and robust excitation sources with added functionality for photoacoustic tomography and microscopy. However, the pulse energy is relatively low.

In conclusion, fiber optic US detection technology is increasingly used in PAI systems, especially for PAE applications, which requires US probes with miniature size and high sensitivity. In PAM and PACT, fiber optic US detection technology is also applied because of its high imaging speed, large field of view, and good sensitivity.

5. Conclusion and future directions

Fiber optic technologies take advantage of the flexibility and compactness of the optical fiber. They have widespread use in different PAI modalities including PAM (OR-PAM, AR-PAM), PACT, and MIPAI (IPA, PAE) configurations for various clinical and pre-clinical applications. In this review article, we overview fiber optic technology utilized in various PAI systems.

Fiber optic technology is mainly categorized as fiber optic light transmission, fiber optic US transmission, and fiber optic US detection. For fiber optic light transmission, we have discussed different fiber optic light transmission systems applied in PAM, PACT and MIPAI. Table 1 and Table 2 summarized these systems. For fiber optic US transmission, we have analyzed various contrast agents and fiber structures in MIPAI (Table 3). For fiber optic US detection, we summarized different fiber optic FP probes in PAE (Table 4). We also studied other types of fiber optic US detection techniques such as FBG US detection, polarization fiber laser, and so on.

In the future, the fiber optic-based PAI system still needs to overcome multiple technical challenges and improve its performance to maximize its clinical application:

(1) **Reduced size and cost of the system**. Currently, Q-switched solid-state lasers and Q-switch pumped OPO systems are mostly used for the light source of the fiber optic-based PAI system. These lasers are bulky and expensive. Laser diodes (LD) and light-emitting diodes (LED) might enable a solution. Future studies can focus on the integration of LD, LED with optical fibers.

(2) **Reduce the light loss through optical fibers**. The light loss of optical fiber mainly occurs in the coupling and transmission of optical fiber. Better coupling methods and small attenuation optical fibers might solve this problem. Furthermore, in some applications, strong light energy might be applied, and such strong fluence may break the glass optical fiber end face. In this case, special optical fibers such as sapphire optical fiber can be utilized in the system.

(3) **Increase the resolution of the system**. Super-resolution (<50 nm) fiber optic-based PAI systems still need to be studied. Some mechanisms could potentially be adapted to improve the fiber optic- based system resolution, such as blind structured illumination [132], multi-speckle illumination [133], and photo-imprint photoacoustic microscopy [134].

(4) **Integrate other biomedical imaging modalities into the system**. PAI can still suffer from low contrast to SNR. The utilization of various imaging modalities could provide more comprehensive target information. Optical coherence tomography (OCT) [135–139], fluorescence [140–142], and hyperspectral microscopy [143] have been integrated into the PAI system to provide additional information. More researches can concentrate on these hybrid technologies.

In summary, fiber optic technologies are at a promising stage of development in the miniaturization and stabilization of PAI systems. We expect fiber optic-based PAI system to find more high-impact applications in biomedical research.

Declaration of Competing Interest

The authors declare that there are no conflicts of interest.

Acknowledgement

We would like to acknowledge the financial support from United States National Institute of Health under DP2 HL137187, R21 AG065776, and R21 DE029025. We also acknowledge the National Science Foundationgrant #1937674.

References

[1] L.V. Wang, S. Hu, Photoacoustic tomography: in vivo imaging from organelles to organs, Science 335 (2012) 1458–1462, https://doi.org/10.1126/science.1216210.
[2] A.B.E. Attia, G. Balasundaram, M. Moothanchery, U.S. Dinish, R. Bi, V. Ntziachristos, M. Olivo, A review of clinical photoacoustic imaging: current and future trends, Photoacoustics 16 (2019) 100144, https://doi.org/10.1016/j.pacs.2019.100144.
[3] I. Steinberg, D.M. Huland, O. Vermesh, H.E. Frostig, W.S. Tummers, S. S. Gambhir, Photoacoustic clinical imaging, Photoacoustics 14 (2019) 77–98, https://doi.org/10.1016/j.pacs.2019.05.001.
[4] S. Manohar, M. Dantuma, Current and future trends in photoacoustic breast imaging, Photoacoustics 16 (2019) 100134, https://doi.org/10.1016/j.pacs.2019.04.004.
[5] S. Jeon, J. Kim, D. Lee, J.W. Baik, C. Kim, Review on practical photoacoustic microscopy, Photoacoustics 15 (2019) 100141, https://doi.org/10.1016/j.pacs.2019.100141.
[6] M. Xu, L.V. Wang, Photoacoustic imaging in biomedicine, Rev. Sci. Instrum. 77 (2006), https://doi.org/10.1063/1.2195024.
[7] A. De La Zerda, C. Zavaleta, S. Keren, S. Vaithilingam, S. Bodapati, Z. Liu, J. Levi, B.R. Smith, T.J. Ma, O. Oralkan, Z. Cheng, X. Chen, H. Dai, B.T. Khuri-Yakub, S. S. Gambhir, Carbon nanotubes as photoacoustic molecular imaging agents in living mice, Nat. Nanotechnol. 3 (2008) 557–562, https://doi.org/10.1038/nnano.2008.231.
[8] S. Mallidi, G.P. Luke, S. Emelianov, Photoacoustic imaging in cancer detection, diagnosis, and treatment guidance, Trends Biotechnol. 29 (2011) 213–221, https://doi.org/10.1016/j.tibtech.2011.01.006.
[9] C. Zhang, K. Maslov, J. Yao, L.V. Wang, In vivo photoacoustic microscopy with 7.6-μm axial resolution using a commercial 125-MHz ultrasonic transducer, J. Biomed. Opt. 17 (2012) 116016, https://doi.org/10.1117/1.jbo.17.11.116016.
[10] S. Hu, L.V. Wang, Photoacoustic imaging and characterization of the microvasculature, J. Biomed. Opt. 15 (2010), 011101, https://doi.org/10.1117/1.3281673.
[11] M. Erfanzadeh, Q. Zhu, Photoacoustic imaging with low-cost sources; a review, Photoacoustics 14 (2019) 1–11, https://doi.org/10.1016/j.pacs.2019.01.004.
[12] K. Pu, A.J. Shuhendler, J.V. Jokerst, J. Mei, S.S. Gambhir, Z. Bao, J. Rao, Semiconducting polymer nanoparticles as photoacoustic molecular imaging probes in living mice, Nat. Nanotechnol. 9 (2014) 233–239, https://doi.org/10.1038/nnano.2013.302.
[13] A. Dragulescu-Andrasi, S.R. Kothapalli, G.A. Tikhomirov, J. Rao, S.S. Gambhir, Activatable oligomerizable imaging agents for photoacoustic imaging of furin-like activity in living subjects, J. Am. Chem. Soc. 135 (2013) 11015–11022, https://doi.org/10.1021/ja4010078.
[14] Y. Jiang, P.K. Upputuri, C. Xie, Z. Zeng, A. Sharma, X. Zhen, J. Li, J. Huang, M. Pramanik, K. Pu, Metabolizable semiconducting polymer nanoparticles for second near-infrared photoacoustic imaging, Adv. Mater. 31 (2019), https://doi.org/10.1002/adma.201808166.
[15] S.K. Kalva, P.K. Upputuri, M. Pramanik, High-speed, low-cost, pulsed-laser-diode-based second-generation desktop photoacoustic tomography system, Opt. Lett. 44 (2019) 81, https://doi.org/10.1364/ol.44.000081.
[16] P. Beard, Biomedical photoacoustic imaging, Interface Focus 1 (2011) 602–631, https://doi.org/10.1098/rsfs.2011.0028.
[17] J. Weber, P.C. Beard, S.E. Bohndiek, Contrast agents for molecular photoacoustic imaging, Nat. Methods 13 (2016) 639–650, https://doi.org/10.1038/nmeth.3929.
[18] A. Hariri, J. Lemaster, J. Wang, A.K.S. Jeevarathinam, D.L. Chao, J.V. Jokerst, The characterization of an economic and portable LED-based photoacoustic imaging system to facilitate molecular imaging, Photoacoustics 9 (2018) 10–20, https://doi.org/10.1016/j.pacs.2017.11.001.
[19] G.P. Luke, D. Yeager, S.Y. Emelianov, Biomedical applications of photoacoustic imaging with exogenous contrast agents, Ann. Biomed. Eng. 40 (2012) 422–437, https://doi.org/10.1007/s10439-011-0449-4.
[20] J.V. Jokerst, A.J. Cole, D. Van De Sompel, S.S. Gambhir, Gold nanorods for ovarian cancer detection with photoacoustic imaging and resection guidance via Raman imaging in living mice, ACS Nano 6 (2012) (2012) 10366–10377, https://doi.org/10.1021/nn304347g.
[21] J.M. Merkes, M. Rueping, F. Kiessling, S. Banala, Photoacoustic detection of superoxide using oxoporphyrinogen and porphyrin, ACS Sens. 4 (2019) 2001–2008, https://doi.org/10.1021/acssensors.9b00224.
[22] K. Pu, J. Mei, J.V. Jokerst, G. Hong, A.L. Antaris, N. Chattopadhyay, A. J. Shuhendler, T. Kurosawa, Y. Zhou, S.S. Gambhir, Z. Bao, J. Rao, Diketopyrrolopyrrole-based semiconducting polymer nanoparticles for in vivo photoacoustic imaging, Adv. Mater. 27 (2015) 5184–5190, https://doi.org/10.1002/adma.201502285.
[23] A.C. Tam, Applications of photoacoustic sensing techniques, Rev. Mod. Phys. 58 (1986) 381–431, https://doi.org/10.1103/RevModPhys.58.381.
[24] L.V. Wang, Multiscale photoacoustic microscopy and computed tomography, Nat. Photonics 3 (2009) 503–509, https://doi.org/10.1038/nphoton.2009.157.
[25] R.A. Kruger, P. Liu, Y.R. Fang, C.R. Appledorn, Photoacoustic ultrasound (PAUS)—reconstruction tomography, Med. Phys. 22 (1995) 1605–1609, https://doi.org/10.1118/1.597429.
[26] H. Vargas, L.C.M. Miranda, Photoacoustic and related photothermal techniques, Phys. Rep. 161 (1988) 43–101, https://doi.org/10.1016/0370-1573(88)90100-7.
[27] B. Cox, J.G. Laufer, S.R. Arridge, P.C. Beard, Quantitative spectroscopic photoacoustic imaging: a review, J. Biomed. Opt. 17 (2012), 061202, https://doi.org/10.1117/1.jbo.17.6.061202.
[28] G. Ku, X. Wang, G. Stoica, L.V. Wang, Multiple-bandwidth photoacoustic tomography, Phys. Med. Biol. 49 (2004) 1329–1338, https://doi.org/10.1088/0031-9155/49/7/018.
[29] J. Yao, L.V. Wang, Sensitivity of photoacoustic microscopy, Photoacoustics 2 (2014) 87–101, https://doi.org/10.1016/j.pacs.2014.04.002.
[30] W. Li, X. Chen, Gold nanoparticles for photoacoustic imaging, Nanomedicine 10 (2015) 299–320, https://doi.org/10.2217/nnm.14.169.
[31] A. de la Zerda, Y.M. Paulus, R. Teed, S. Bodapati, Y. Dollberg, B.T. Khuri-Yakub, M.S. Blumenkranz, D.M. Moshfeghi, S.S. Gambhir, Photoacoustic ocular imaging, Opt. Lett. 35 (2010) 270–272, https://doi.org/10.1364/ol.35.000270.
[32] A. Rosencwaig, Photoacoustic spectroscopy, Annu. Rev. Biophys. Bioeng. 9 (1980) 31–54, https://doi.org/10.1146/annurev.bb.09.060180.000335.
[33] S. Jiao, M. Jiang, J. Hu, A. Fawzi, Q. Zhou, K.K. Shung, C.A. Puliafito, H.F. Zhang, Photoacoustic ophthalmoscopy for in vivo retinal imaging, Opt. Express 18 (2010) 3967–3972, https://doi.org/10.1364/oe.18.003967.
[34] Z. Xie, S. Jiao, H.F. Zhang, C.A. Puliafito, Laser-scanning optical-resolution photoacoustic microscopy, Opt. Lett. 34 (2009) 1771–1773, https://doi.org/10.1364/ol.34.001771.
[35] K. Jansen, A.F. van der Steen, M. Wu, H.M. van Beusekom, G. Springeling, X. Li, Q. Zhou, K. Kirk Shung, D.P. de Kleijn, G. van Soest, Spectroscopic intravascular photoacoustic imaging of lipids in atherosclerosis, J. Biomed. Opt. 19 (2014), 026006, https://doi.org/10.1117/1.jbo.19.2.026006.

[36] T. Zhao, A.E. Desjardins, S. Ourselin, T. Vercauteren, W. Xia, Minimally invasive photoacoustic imaging: current status and future perspectives, Photoacoustics. 16 (2019) 100146, https://doi.org/10.1016/j.pacs.2019.100146.

[37] J. Yao, L.V. Wang, Photoacoustic tomography: fundamentals, advances and prospects, Contrast Media Mol. Imaging 6 (2011) 332–345, https://doi.org/10.1002/cmmi.443.

[38] J. Xia, Y. Wang, H. Wan, Recent progress in multimodal photoacoustic tomography, X-Acoustics Imaging Sens. 1 (2015), https://doi.org/10.1515/phto-2015-0008.

[39] L.V. Wang, J. Yao, A practical guide to photoacoustic tomography in the life sciences, Nat. Methods 13 (2016) 627–638, https://doi.org/10.1038/nmeth.3925.

[40] A. Fatima, K. Kratkiewicz, R. Manwar, M. Zafar, R. Zhang, B. Huang, N. Dadashzadeh, J. Xia, K. (Mohammad) Avanaki, Review of cost reduction methods in photoacoustic computed tomography, Photoacoustics 15 (2019) 100137, https://doi.org/10.1016/j.pacs.2019.100137.

[41] V.G. Peters, D.R. Wyman, M.S. Patterson, G.L. Frank, Optical properties of normal and diseased human breast tissues in the visible and near infrared, Phys. Med. Biol. 35 (1990) 1317–1334, https://doi.org/10.1088/0031-9155/35/9/010.

[42] U. Chitgupi, N. Nyayapathi, J. Kim, D. Wang, B. Sun, C. Li, K. Carter, W.C. Huang, C. Kim, J. Xia, J.F. Lovell, Surfactant-stripped micelles for NIR-II photoacoustic imaging through 12 cm of breast tissue and whole human breasts, Adv. Mater. 31 (2019) 1902279, https://doi.org/10.1002/adma.201902279.

[43] B. Wang, J.L. Su, J. Amirian, S.H. Litovsky, R. Smalling, S. Emelianov, Detection of lipid in atherosclerotic vessels using ultrasound-guided spectroscopic intravascular photoacoustic imaging, Opt. Express 18 (2010) 4889–4897, https://doi.org/10.1364/oe.18.004889.

[44] P. Wang, T. Ma, M.N. Slipchenko, S. Liang, J. Hui, K.K. Shung, S. Roy, M. Sturek, Q. Zhou, Z. Chen, J.X. Cheng, High-speed intravascular photoacoustic imaging of lipid-laden atherosclerotic plaque enabled by a 2-kHz Barium Nitrite Raman Laser, Sci. Rep. 4 (2014) 6889, https://doi.org/10.1038/srep06889.

[45] W. Xia, D.I. Nikitichev, J.M. Mari, S.J. West, R. Pratt, A.L. David, S. Ourselin, P. C. Beard, A.E. Desjardins, Performance characteristics of an interventional multispectral photoacoustic imaging system for guiding minimally invasive procedures, J. Biomed. Opt. 20 (2015), 086005, https://doi.org/10.1117/1.jbo.20.8.086005.

[46] B. Wang, J.L. Su, A.B. Karpiouk, K.V. Sokolov, R.W. Smalling, S.Y. Emelianov, Intravascular photoacoustic imaging, IEEE J. Sel. Top. Quantum Electron. 16 (2010) 588–599, https://doi.org/10.1109/JSTQE.2009.2037023.

[47] D. Piras, C. Grijsen, P. Schütte, W. Steenbergen, S. Manohar, Photoacoustic needle: minimally invasive guidance to biopsy, J. Biomed. Opt. 18 (2013), 070502, https://doi.org/10.1117/1.jbo.18.7.070502.

[48] Bo Wang, Stanislav Emelianov, "Thermal intravascular photoacoustic imaging" Biomedical optics express 2, no. 11 (2011): 3072-3078. B. Wang, S. Emelianov, Thermal intravascular photoacoustic imaging, Biomed. Opt. Express 2 (2011) 3072–3078, https://doi.org/10.1364/boe.2.003072.

[49] K. Jansen, A.F.W. van der Steen, H.M.M. van Beusekom, J.W. Oosterhuis, G. van Soest, Intravascular photoacoustic imaging of human coronary atherosclerosis, Opt. Lett. 36 (2011) 597–599, https://doi.org/10.1364/ol.36.000597.

[50] S. Sethuraman, S.R. Aglyamov, J.H. Amirian, R.W. Smalling, S.Y. Emelianov, Intravascular photoacoustic imaging using an IVUS imaging catheter, IEEE Trans. Ultrason. Ferroelectr. Freq. Control 54 (2007) 978–986, https://doi.org/10.1109/TUFFC.2007.343.

[51] Y. Cao, J. Hui, A. Kole, P. Wang, Q. Yu, W. Chen, M. Sturek, J.X. Cheng, High-sensitivity intravascular photoacoustic imaging of lipid-laden plaque with a collinear catheter design, Sci. Rep. 6 (2016) 1–8, https://doi.org/10.1038/srep25236.

[52] E.Z. Zhang, P.C. Beard, Characteristics of optimized fibre-optic ultrasound receivers for minimally invasive photoacoustic detection, Photons Plus Ultrasound Imaging Sens. 9323 (2015) 932311, https://doi.org/10.1117/12.2081904.

[53] S. Noimark, R.J. Colchester, B.J. Blackburn, E.Z. Zhang, E.J. Alles, S. Ourselin, P. C. Beard, I. Papakonstantinou, I.P. Parkin, A.E. Desjardins, Carbon-nanotube-PDMS composite coatings on optical fibers for all-optical ultrasound imaging, Adv. Funct. Mater. 26 (2016) 8390–8396, https://doi.org/10.1002/adfm.201601337.

[54] M.T. Graham, J. Huang, F. Creighton, M.A.L. Bell, Simulations and human cadaver head studies to identify optimal acoustic receiver locations for minimally invasive photoacoustic-guided neurosurgery, Photoacoustics (2020) 100183, https://doi.org/10.1016/j.pacs.2020.100183.

[55] B. Eddins, M.A. Lediju Bell, Optimizing light delivery for a photoacoustic surgical system, Photons Plus Ultrasound Imaging Sens. 10064 (2017) 100640J, https://doi.org/10.1117/12.2253521.

[56] K. Sivasubramanian, V. Periyasamy, K.K. Wen, M. Pramanik, Optimizing light delivery through fiber bundle in photoacoustic imaging with clinical ultrasound system: Monte Carlo simulation and experimental validation, J. Biomed. Opt. 22 (2016) 041008, https://doi.org/10.1117/1.jbo.22.4.041008.

[57] A. Dangi, S. Agrawal, G.R. Datta, V. Srinivasan, S.-R. Kothapalli, Towards a low-cost and portable photoacoustic microscope for point-of-care and wearable applications, IEEE Sens. J. (2019), https://doi.org/10.1109/jsen.2019.2935684.

[58] V. Periyasamy, M. Pramanik, Monte Carlo simulation of light transport in tissue for optimizing light delivery in photoacoustic imaging of the sentinel lymph node, J. Biomed. Opt. 18 (2013) 106008, https://doi.org/10.1117/1.jbo.18.10.106008.

[59] M.A. Lediju Bell, A.K. Ostrowski, K. Li, P. Kazanzides, E.M. Boctor, Localization of transcranial targets for photoacoustic-guided endonasal surgeries, Photoacoustics 3 (2015) 78–87, https://doi.org/10.1016/j.pacs.2015.05.002.

[60] P.K. Upputuri, M. Pramanik, Recent advances toward preclinical and clinical translation of photoacoustic tomography: a review, J. Biomed. Opt. 22 (2016), 041006, https://doi.org/10.1117/1.jbo.22.4.041006.

[61] M. Graham, F. Assis, D. Allman, A. Wiacek, E. Gonzalez, M. Gubbi, J. Dong, H. Hou, S. Beck, J. Chrispin, M. Bell, Photoacoustic image guidance and robotic visual servoing to mitigate fluoroscopy during cardiac catheter interventions, in: Advanced Biomedical and Clinical Diagnostic and Surgical Guidance Systems XVIII, 11229, 2020, p. 112291E, https://doi.org/10.1117/12.2546910.

[62] E. Brown, J. Brunker, S.E. Bohndiek, Photoacoustic imaging as a tool to probe the tumour microenvironment, DMM Dis, Model. Mech. 12 (2019), https://doi.org/10.1242/dmm.039636.

[63] A. Dangi, S. Agrawal, S. Tiwari, S. Jadhav, C. Cheng, G.R. Datta, S. Troiler-McKinstry, R. Pratap, S.-R. Kothapalli, Ring PMUT array based miniaturized photoacoustic endoscopy device, Photons Plus Ultrasound Imaging Sens. 10878 (2019) 1087811, https://doi.org/10.1117/12.2510000.

[64] L. Lin, J. Xia, T.T.W. Wong, L. Li, L.V. Wang, In vivo deep brain imaging of rats using oral-cavity illuminated photoacoustic computed tomography, J. Biomed. Opt. 20 (2015), 016019, https://doi.org/10.1117/1.jbo.20.1.016019.

[65] M.K.A. Singh, V. Parameshwarappa, E. Hendriksen, W. Steenbergen, S. Manohar, Photoacoustic-guided focused ultrasound for accurate visualization of brachytherapy seeds with the photoacoustic needle, J. Biomed. Opt. 21 (2016) 120501, https://doi.org/10.1117/1.jbo.21.12.120501.

[66] M. Ai, J. Youn, S.E. Salcudean, R. Rohling, P. Abolmaesumi, S. Tang, Photoacoustic tomography for imaging the prostate: a transurethral illumination probe design and application, Biomed. Opt. Express 10 (2019) 2588–2605, https://doi.org/10.1364/boe.10.002588.

[67] B. Bungart, Y. Cao, T. Yang-Tran, S. Gorsky, L. Lan, D. Roblyer, M.O. Koch, L. Cheng, T. Masterson, J.-X. Cheng, Cylindrical illumination with angular coupling for whole-prostate photoacoustic tomography, Biomed. Opt. Express 10 (2019) 1405–1419, https://doi.org/10.1364/boe.10.001405.

[68] K.J. Francis, E. Rascevska, S. Manohar, Photoacoustic imaging assisted radiofrequency ablation: illumination strategies and prospects, in: IEEE Reg. 10 Annu. Int. Conf. Proceedings/TENCON, 2019, 2019, pp. 118–122, https://doi.org/10.1109/TENCON.2019.8929646.

[69] K. Xiong, S. Yang, X. Li, D. Xing, Autofocusing optical-resolution photoacoustic endoscopy, Opt. Lett. 43 (2018) 1846–1849, https://doi.org/10.1364/ol.43.001846.

[70] J.-M. Yang, K. Maslov, H.-C. Yang, Q. Zhou, K.K. Shung, L.V. Wang, Photoacoustic endoscopy, Opt. Lett. 34 (2009) 1591–1593, https://doi.org/10.1364/ol.34.001591.

[71] J.-M. Yang, R. Chen, C. Favazza, J. Yao, C. Li, Z. Hu, Q. Zhou, K.K. Shung, L. V. Wang, A 2.5-mm diameter probe for photoacoustic and ultrasonic endoscopy, Opt. Express 20 (2012) 23944–23953, https://doi.org/10.1364/oe.20.023944.

[72] Y. Qu, C. Li, J. Shi, Transvaginal fast-scanning optical-resolution photoacoustic endoscopy, J. Biomed. Opt. 23 (2018) 121617, https://doi.org/10.1117/1.jbo.23.12.121617.

[73] M. Basij, Y. Yan, S.S. Alshahrani, H. Helmi, T.K. Burton, J.W. Burmeister, M. M. Dominello, I.S. Winer, M. Mehrmohammadi, Miniaturized phased-array ultrasound and photoacoustic endoscopic imaging system, Photoacoustics 15 (2019) 100139, https://doi.org/10.1016/j.pacs.2019.100139.

[74] D. Cai, G. Li, D. Xia, Z. Li, Z. Guo, S.-L. Chen, Synthetic aperture focusing technique for photoacoustic endoscopy, Opt. Express 25 (2017) 20162–20171, https://doi.org/10.1364/oe.25.020162.

[75] L. Vionnet, J. Gateau, M. Schwarz, A. Buehler, V. Ermolayev, V. Ntziachristos, 24-MHz scanner for optoacoustic imaging of skin and burn, IEEE Trans. Med. Imaging 33 (2014) 535–545, https://doi.org/10.1109/TMI.2013.2289930.

[76] A. Taruttis, G.M. Van Dam, V. Ntziachristos, Mesoscopic and macroscopic optoacoustic imaging of cancer, Cancer Res. 75 (2015) 1548–1559, https://doi.org/10.1158/0008-5472.CAN-14-2522.

[77] A. Taruttis, A.C. Timmermans, P.C. Wouters, M. Kacprowicz, G.M. Van Dam, V. Ntziachristos, Optoacoustic imaging of human vasculature: feasibility by using a handheld probe, Radiology 281 (2016) 256–263, https://doi.org/10.1148/radiol.2016152160.

[78] X.L. Deán-Ben, S. Gottschalk, B. Mc Larney, S. Shoham, D. Razansky, Advanced optoacoustic methods for multiscale imaging of: in vivo dynamics, Chem. Soc. Rev. 46 (2017) 2158–2198, https://doi.org/10.1039/c6cs00765a.

[79] W. Choi, E.Y. Park, S. Jeon, C. Kim, Clinical photoacoustic imaging platforms, Biomed. Eng. Lett. 8 (2018) 139–155, https://doi.org/10.1007/s13534-018-0062-7.

[80] N. Wu, X. Zou, J. Zhou, X. Wang, Fiber optic ultrasound transmitters and their applications, Meas. J. Int. Meas. Confed. 79 (2016) 164–171, https://doi.org/10.1016/j.measurement.2015.10.002.

[81] E.Z. Zhang, P.C. Beard, A miniature all-optical photoacoustic imaging probe, Photons Plus Ultrasound Imaging Sens. 7899 (2011) 78991F, https://doi.org/10.1117/12.874883.

[82] W. Xing, L. Wang, K. Maslov, L.V. Wang, Integrated optical- and acoustic-resolution photoacoustic microscopy based on an optical fiber bundle, Opt. Lett. 38 (2013) 52–54, https://doi.org/10.1364/ol.38.000052.

[83] D. Piras, C. Grijsen, P. Schütte, W. Steenbergen, S. Manohar, Photoacoustic needle: minimally invasive guidance to biopsy, J. Biomed. Opt. 18 (2013), 070502, https://doi.org/10.1117/1.jbo.18.7.070502.

[84] T. Zhao, L. Su, W. Xia, Optical ultrasound generation and detection for intravascular imaging: a review, J. Healthc. Eng. (2018), https://doi.org/10.1155/2018/3182483.

[85] T. Buma, M. Spisar, M. O'Donnell, High-frequency ultrasound array element using thermoelastic expansion in an elastomeric film, Appl. Phys. Lett. 79 (2001) 548–550, https://doi.org/10.1063/1.1388027.
[86] P.A. Fomitchov, A.K. Kromine, S. Krishnaswamy, Photoacoustic probes for nondestructive testing and biomedical applications, Appl. Opt. 41 (2002) 4451–4459, https://doi.org/10.1364/ao.41.004451.
[87] H. Won Baac, J.G. Ok, H.J. Park, T. Ling, S.L. Chen, A.J. Hart, L.J. Guo, Carbon nanotube composite optoacoustic transmitters for strong and high frequency ultrasound generation, Appl. Phys. Lett. 97 (2010) 234104, https://doi.org/10.1063/1.3522833.
[88] B.Y. Hsieh, J. Kim, J. Zhu, S. Li, X. Zhang, X. Jiang, A laser ultrasound transducer using carbon nanofibers-polydimethylsiloxane composite thin film, Appl. Phys. Lett. 106 (2015), 021902, https://doi.org/10.1063/1.4905659.
[89] J. Zhou, N. Wu, X. Wang, Y. Liu, T. Ma, D. Coxe, C. Cao, Water temperature measurement using a novel fiber optic ultrasound transducer system, in: 2015 IEEE Int. Conf. Inf. Autom. ICIA 2015 - Conjunction with 2015 IEEE Int. Conf. Autom. Logist., 2015, 2015, pp. 2316–2319, https://doi.org/10.1109/ICInfA.2015.7279672.
[90] J. Zhou, N. Wu, S. Bi, X. Wang, Ultrasound generation from an optical fiber sidewall, in: Sensors Smart Struct. Technol. Civil, Mech. Aerosp. Syst., 9803, 2016, p. 98031U, https://doi.org/10.1117/12.2219008.
[91] T. Yoshino, T. Ose, K. Kurosawa, K. Itoh, Fiber-optic Fabry–Perot Interferometer and its sensor applications, IEEE Trans. Microw. Theory Tech. 30 (1982) 1612–1621, https://doi.org/10.1109/TMTT.1982.1131298.
[92] X. Guo, J. Zhou, C. Du, X. Wang, Optical Fiber ultrasound probe for radiofrequency ablation temperature monitoring: in-vitro results, IEEE Photonics Technol. Lett. 32 (2020) 689–692, https://doi.org/10.1109/LPT.2020.2991720.
[93] H. Grün, T. Berer, P. Burgholzer, R. Nuster, G. Paltauf, Three-dimensional photoacoustic imaging using fiber-based line detectors, J. Biomed. Opt. 15 (2010), 021306, https://doi.org/10.1117/1.3381186.
[94] Y. Liang, J. Liu, L. Jin, B.-O. Guan, L. Wang, Fast-scanning photoacoustic microscopy with a side-looking fiber optic ultrasound sensor, Biomed. Opt. Express 9 (2018) 5809–5816, https://doi.org/10.1364/boe.9.005809.
[95] K. Park, J.Y. Kim, C. Lee, S. Jeon, G. Lim, C. Kim, Handheld photoacoustic microscopy probe, Sci. Rep. 7 (2017) 1–15, https://doi.org/10.1038/s41598-017-13224-3.
[96] I.N. Papadopoulos, O. Simandoux, S. Farahi, J. Pierre Huignard, E. Bossy, D. Psaltis, C. Moser, Optical-resolution photoacoustic microscopy by use of a multimode fiber, Appl. Phys. Lett. 102 (2013) 211106, https://doi.org/10.1063/1.4807621.
[97] A. Garcia-Uribe, T.N. Erpelding, A. Krumholz, H. Ke, K. Maslov, C. Appleton, J. A. Margenthaler, L.V. Wang, Dual-Modality photoacoustic and ultrasound imaging system for noninvasive sentinel lymph node detection in patients with breast cancer, Sci. Rep. 5 (2015) 15748, https://doi.org/10.1038/srep15748.
[98] M. Moothanchery, R. Bi, J.Y. Kim, S. Jeon, C. Kim, M. Olivo, Optical resolution photoacoustic microscopy based on multimode fibers, Biomed. Opt. Express 9 (2018) 1190–1197, https://doi.org/10.1364/boe.9.001190.
[99] P. Hajireza, W. Shi, R.J. Zemp, Label-free in vivo fiber-based optical-resolution photoacoustic microscopy, Opt. Lett. 36 (2011) 4107–4109, https://doi.org/10.1364/ol.36.004107.
[100] J. Baik, J.Y. Kim, S. Cho, S. Choi, J. Kim, C. Kim, Ultrawide-field acoustic-resolution photoacoustic microscopy, Photons Plus Ultrasound: Imaging and Sensing 10878 (2019) 1087815, https://doi.org/10.1117/12.2507614.
[101] X. Cai, B.S. Paratala, S. Hu, B. Sitharaman, L.V. Wang, Multiscale photoacoustic microscopy of single-walled carbon nanotube-incorporated tissue engineering scaffolds, Tissue Eng. - Part C Methods 18 (2012) 310–317, https://doi.org/10.1089/ten.tec.2011.0519.
[102] M. Moothanchery, R. Bi, J.Y. Kim, G. Balasundaram, C. Kim, M. Olivo, High-speed simultaneous multiscale photoacoustic microscopy, J. Biomed. Opt. 24 (2019), 086001, https://doi.org/10.1117/1.jbo.24.8.086001.
[103] M.A. Lediju Bell, J. Shubert, Photoacoustic-based visual servoing of a needle tip, Sci. Rep. 8 (2018) 1–12, https://doi.org/10.1038/s41598-018-33931-9.
[104] M. Li, B. Lan, W. Liu, J. Xia, J. Yao, Internal-illumination photoacoustic computed tomography, J. Biomed. Opt. 23 (2018), 030506, https://doi.org/10.1117/1.jbo.23.3.030506.
[105] W. Wei, X. Li, Q. Zhou, K.K. Shung, Z. Chen, Integrated ultrasound and photoacoustic probe for co-registered intravascular imaging, J. Biomed. Opt. 16 (2011) 106001, https://doi.org/10.1117/1.3631798.
[106] Y. Zhang, Y. Cao, J.-X. Cheng, High-resolution photoacoustic endoscope through beam self-cleaning in a graded index fiber, Opt. Lett. 44 (2019) 3841–3844, https://doi.org/10.1364/ol.44.003841.
[107] R.J. Colchester, C.A. Mosse, D.S. Bhachu, J.C. Bear, C.J. Carmalt, I.P. Parkin, B. E. Treeby, I. Papakonstantinou, A.E. Desjardins, Laser-generated ultrasound with optical fibres using functionalised carbon nanotube composite coatings, Appl. Phys. Lett. 104 (2014) 173502, https://doi.org/10.1063/1.4873678.
[108] X. Zou, N. Wu, Y. Tian, X. Wang, Broadband miniature fiber optic ultrasound generator, Opt. Express 22 (2014) 18119–18127, https://doi.org/10.1364/oe.22.018119.
[109] R.K. Poduval, S. Noimark, R.J. Colchester, T.J. Macdonald, I.P. Parkin, A. E. Desjardins, I. Papakonstantinou, Optical fiber ultrasound transmitter with electrospun carbon nanotube-polymer composite, Appl. Phys. Lett. 110 (2017) 223701, https://doi.org/10.1063/1.4984838.
[110] E. Vannacci, L. Belsito, F. Mancarella, M. Ferri, G.P. Veronese, A. Roncaglia, E. Biagi, Miniaturized fiber-optic ultrasound probes for endoscopic tissue analysis by micro-opto-mechanical technology, Biomed. Microdevices 16 (2014) 415–426, https://doi.org/10.1007/s10544-014-9844-6.
[111] W.-Y. Chang, W. Huang, J. Kim, S. Li, X. Jiang, Candle soot nanoparticles-polydimethylsiloxane composites for laser ultrasound transducers, Appl. Phys. Lett. 107 (2015) 161903, https://doi.org/10.1063/1.4934587.
[112] R.J. Colchester, E.J. Alles, A.E. Desjardins, A directional fibre optic ultrasound transmitter based on a reduced graphene oxide and polydimethylsiloxane composite, Appl. Phys. Lett. 114 (2019) 113505, https://doi.org/10.1063/1.5089750.
[113] J. Zhou, X. Guo, C. Du, X. Wang, Ultrasound beam steering using a fiber optic ultrasound phased array, Opt. Lett. 44 (2019) 5390–5393, https://doi.org/10.1364/ol.44.005390.
[114] J. Zhou, X. Guo, C. Du, N. Wu, X. Wang, Characterization of ultrasonic generation from a fiber-optic sidewall, Fiber Optic Sens. Appl. XV 10654 (2018) 106540U, https://doi.org/10.1117/12.2303890.
[115] Y. Li, J. Tian, S. Ji, C. Zhou, Y. Sun, Y. Yao, Fiber-optic multipoint laser-ultrasonic excitation transducer using coreless fibers, Opt. Express 27 (2019) 6116–6128, https://doi.org/10.1364/oe.27.006116.
[116] E.J. Alles, E. J, S. Noimark, E. Zhang, P.C. Beard, A.E. Desjardins, Pencil beam all-optical ultrasound imaging, Biomed. Opt. Express 7 (2016) 3696, https://doi.org/10.1364/boe.7.003696.
[117] R.J. Colchester, E.Z. Zhang, C.A. Mosse, P.C. Beard, I. Papakonstantinou, A. E. Desjardins, Broadband miniature optical ultrasound probe for high resolution vascular tissue imaging, Biomed. Opt. Express 6 (2015) 1502–1511, https://doi.org/10.1364/boe.6.001502.
[118] S. Noimark, R.J. Colchester, R.K. Poduval, E. Maneas, E.J. Alles, T. Zhao, E. Z. Zhang, M. Ashworth, E. Tsolaki, A.H. Chester, N. Latif, S. Bertazzo, A.L. David, S. Ourselin, P.C. Beard, I.P. Parkin, I. Papakonstantinou, A.E. Desjardins, Polydimethylsiloxane composites for optical ultrasound generation and multimodality imaging, Adv. Funct. Mater. 28 (2018) 1704919, https://doi.org/10.1002/adfm.201704919.
[119] G. Li, Z. Guo, S.-L. Chen, Miniature all-optical probe for large synthetic aperture photoacoustic-ultrasound imaging, Opt. Express 25 (2017) 25023–25035, https://doi.org/10.1364/oe.25.025023.
[120] R.J. Colchester, C. Little, G. Dwyer, S. Noimark, E.J. Alles, E.Z. Zhang, C.D. Loder, I.P. Parkin, I. Papakonstantinou, P.C. Beard, M.C. Finlay, R.D. Rakhit, A. E. Desjardins, All-optical rotational ultrasound imaging, Sci. Rep. 9 (2019) 55–76, https://doi.org/10.1038/s41598-019-41970-z.
[121] B.-Y. Hsieh, S.-L. Chen, T. Ling, L.J. Guo, P.-C. Li, All-optical scanhead for ultrasound and photoacoustic imaging-Imaging mode switching by dichroic filtering, Photoacoustics 2 (2014) 39–46, https://doi.org/10.1016/j.pacs.2013.12.002.
[122] W. Xia, C.A. Mosse, R.J. Colchester, J.M. Mari, D.I. Nikitichev, S.J. West, S. Ourselin, P.C. Beard, A.E. Desjardins, Fiber optic photoacoustic probe with ultrasonic tracking for guiding minimally invasive procedures. Opt. InfoBase Conf. Pap., 2014, p. 95390K, https://doi.org/10.1117/12.2182647.
[123] R. Ansari, E.Z. Zhang, A.E. Desjardins, P.C. Beard, All-optical forward-viewing photoacoustic probe for high-resolution 3D endoscopy, Light Sci. Appl. 7 (2018) 1–9, https://doi.org/10.1038/s41377-018-0070-5.
[124] Y. Miida, Y. Matsuura, All-optical photoacoustic imaging system using fiber ultrasound probe and hollow optical fiber bundle, Opt. Express 21 (2013) 22023–22033, https://doi.org/10.1364/oe.21.022023.
[125] M.C. Finlay, C.A. Mosse, R.J. Colchester, S. Noimark, E.Z. Zhang, S. Ourselin, P. C. Beard, R.J. Schillin, I.P. Parkin, I. Papakonstantinou, A.E. Desjardins, Through-needle all-optical ultrasound imaging in vivo: a preclinical swine study, Light Sci. Appl. 6 (2017), https://doi.org/10.1038/lsa.2017.103 e17103-e17103.
[126] E.J. Alles, N. Fook Sheung, S. Noimark, E.Z. Zhang, P.C. Beard, A.E. Desjardins, A reconfigurable all-optical ultrasound transducer array for 3D endoscopic imaging, Sci. Rep. 7 (2017) 1–9, https://doi.org/10.1038/s41598-017-01375-2.
[127] J. Zhou, R. Shah, X. Guo, C. Du, X. Wang, All-optical fiber ultrasound imaging system based on the photoacoustic principle, in: Medical Imaging 2020: Ultrasonic Imaging and Tomography, 11319, 2020, p. 1131915, https://doi.org/10.1117/12.2564494.
[128] Y. Liang, L. Jin, L. Wang, X. Bai, L. Cheng, B.O. Guan, Fiber-laser-based ultrasound sensor for photoacoustic imaging, Sci. Rep. 7 (2017) 40849, https://doi.org/10.1038/srep40849.
[129] R. Shnaiderman, G. Wissmeyer, M. Seeger, D. Soliman, H. Estrada, D. Razansky, A. Rosenthal, V. Ntziachristos, Fiber interferometer for hybrid optical and optoacoustic intravital microscopy, Optica 4 (2017) 1180–1187, https://doi.org/10.1364/optica.4.001180.
[130] H. Li, B. Dong, Z. Zhang, H.F. Zhang, C. Sun, A transparent broadband ultrasonic detector based on an optical micro-ring resonator for photoacoustic microscopy, Sci. Rep. 4 (2015) 4496, https://doi.org/10.1038/srep04496.
[131] T.J. Allen, M.O. Berendt, J. Spurrell, S.U. Alam, E.Z. Zhang, D.J. Richardson, P. C. Beard, Novel fibre lasers as excitation sources for photoacoustic tomography and microscopy, Photons Plus Ultrasound: Imaging and Sensing 9708 (2016) 97080W, https://doi.org/10.1117/12.2211733.
[132] T.W. Murray, M. Haltmeier, T. Berer, E. Leiss-Holzinger, P. Burgholzer, Super-resolution photoacoustic microscopy using blind structured illumination, Optica 4 (2017) 17–22, https://doi.org/10.1364/optica.4.000017.
[133] A.M. Caravaca-Aguirre, S. Singh, S. Labouesse, M.V. Baratta, R. Piestun, E. Bossy, Hybrid photoacoustic-fluorescence microendoscopy through a multimode fiber using speckle illumination, Apl Photonics 4 (2019), 096103, https://doi.org/10.1063/1.5113476.
[134] J. Yao, L. Wang, C. Li, C. Zhang, L.V. Wang, Photoimprint photoacoustic microscopy for three-dimensional label-free subdiffraction imaging, Phys. Rev. Lett. 112 (2014) 014302, https://doi.org/10.1103/PhysRevLett.112.014302.

[135] E.Z. Zhang, B. Povazay, J. Laufer, A. Alex, B. Hofer, B. Pedley, C. Glittenberg, B. Treeby, B. Cox, P. Beard, W. Drexler, Multimodal photoacoustic and optical coherence tomography scanner using an all optical detection scheme for 3D morphological skin imaging, Biomed. Opt. Express 2 (2011) 2202–2215, https://doi.org/10.1364/boe.2.002202.
[136] Y. Yang, X. Li, T. Wang, P.D. Kumavor, A. Aguirre, K.K. Shung, Q. Zhou, M. Sanders, M. Brewer, Q. Zhu, Integrated optical coherence tomography, ultrasound and photoacoustic imaging for ovarian tissue characterization, Biomed. Opt. Express 2 (2011) 2551–2561, https://doi.org/10.1364/boe.2.002551.
[137] T. Liu, Q. Wei, J. Wang, S. Jiao, H.F. Zhang, Combined photoacoustic microscopy and optical coherence tomography can measure metabolic rate of oxygen, Biomed. Opt. Express 2 (2011) 1359–1365, https://doi.org/10.1364/boe.2.001359.
[138] S.J. Mathews, C. Little, C.D. Loder, R.D. Rakhit, W. Xia, E.Z. Zhang, P.C. Beard, M. C. Finlay, A.E. Desjardins, All-optical dual photoacoustic and optical coherence tomography intravascular probe, Photoacoustics 11 (2018) 65–70, https://doi.org/10.1016/j.pacs.2018.07.002.
[139] T. Berer, E. Leiss-Holzinger, A. Hochreiner, J. Bauer-Marschallinger, A. Buchsbaum, Multimodal noncontact photoacoustic and optical coherence tomography imaging using wavelength-division multiplexing, J. Biomed. Opt. 20 (2015), 046013, https://doi.org/10.1117/1.jbo.20.4.046013.
[140] P. Shao, W. Shi, P. Hajireza, R.J. Zemp, Integrated micro-endoscopy system for simultaneous fluorescence and optical-resolution photoacoustic imaging, J. Biomed. Opt. 17 (2012), 076024, https://doi.org/10.1117/1.jbo.17.7.076024.
[141] S.L. Chen, Z. Xie, L.J. Guo, X. Wang, A fiber-optic system for dual-modality photoacoustic microscopy and confocal fluorescence microscopy using miniature components, Photoacoustics 1 (2013) 30–35, https://doi.org/10.1016/j.pacs.2013.07.001.
[142] L. Xi, G. Zhou, N. Gao, L. Yang, D.A. Gonzalo, S.J. Hughes, H. Jiang, Photoacoustic and fluorescence image-guided surgery using a multifunctional targeted nanoprobe, Ann. Surg. Oncol. 21 (2014) 1602–1609, https://doi.org/10.1245/s10434-014-3541-9.
[143] N. Liu, Z. Chen, D. Xing, Integrated photoacoustic and hyperspectral dual modality microscope for co-imaging of melanoma and cutaneous squamous cell carcinoma in vivo, J. Biophotonics (2020) e202000105, https://doi.org/10.1002/jbio.202000105.

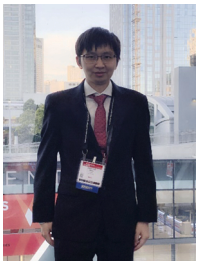

Jingcheng Zhou: Jingcheng Zhou is now a Postdoctoral researcher with Dr. Jokerst Bioimaging Lab in the Nanoengineering department at the UC San Diego. He received his Ph.D. degree in Biomedical Engineering and Biotechnology with Xingwei Wang at UMass Lowell. He got his M.S. degree in Electrical Engineering from the University of Bridgeport and a B.S. degree in Electronic Information Engineering from Wuhan University of Technology Huaxia College. He is currently working on building heparin-sensitive acoustic fibers and technologies to quantitate anticoagulants.

Jesse V. Jokerst: Jesse V. Jokerst completed a B.S. cum laude at Truman State University. After a Ph.D. in Chemistry at UT Austin with John McDevitt, he completed a postdoc with Sam Gambhir in Stanford Radiology. Now an Associate Professor in the Department of Nanoengineering at UC San Diego, the Jokerst group is eager to collaborate on projects broadly related to human health and nanotechnology.